

Unravelling links between squid catch variations and biophysical mechanisms in South African waters

Fatma Jebri^{a,*}, Dionysios E. Raitzos^{b,c}, John A. Gittings^{b,d}, Zoe L. Jacobs^a, Meric Srokosz^a, Jessica Gornall^e, Warwick H.H. Sauer^e, Michael J. Roberts^{a,f}, Ekaterina Popova^a

^a National Oceanography Centre, Southampton, SO14 3ZH, United Kingdom

^b Department of Biology, National and Kapodistrian University of Athens, Athens, Greece

^c Plymouth Marine Laboratory, Plymouth, PL1 3DH, United Kingdom

^d Department of Earth Science and Engineering, King Abdullah University of Science and Technology, Thuwal, Saudi Arabia

^e Department of Ichthyology and Fisheries Science, Rhodes University, Makhanda, South Africa

^f Nelson Mandela University, Ocean Science and Marine Food Security, Gqeberha, 6001, South Africa

ARTICLE INFO

Keywords:

Squid catch
Wind-driven upwelling
Remote sensing
Chlorophyll-a
Phytoplankton phenology
South african shelf

ABSTRACT

Using satellite observations, this study uncovers the biophysical drivers of the lucrative chokka squid fishery in South Africa over the last two decades (1998–2017) and addresses their potential links with low squid catches. Chokka squid fishing is crucial to the economic wellbeing of local communities. However, the squid biomass is prone to considerable fluctuations, including abrupt declines with negative socio-economic impacts. We show that the squid catch is significantly and positively correlated with satellite-derived chlorophyll-*a* (*Chl-a*, an index of phytoplankton biomass) from year to year in South African coastal waters. Two main phytoplankton blooms are observed to occur seasonally in the austral spring and autumn, peaking in October and April, respectively. From October to April, phytoplankton abundance is influenced by the occurrence of wind-driven upwelling over the South African west coast (southern Benguela) and the central Agulhas Bank (so-called Cold Ridge upwelling), while the surface currents appear more important for shelf edge processes and advection along the Cold Ridge on shorter timescales. Low squid catches are observed in 2001 and 2013 and linked to declines in *Chl-a* induced by weak winds and relaxed negative wind stress curl over the southwest coast in 2001, and over the southwest coast and the central Agulhas Bank in 2013. Phytoplankton phenology (bloom timing) analysis reveals absent, or shorter and delayed blooms, over the Benguela upwelling region in 2001 and both the Benguela and Cold Ridge upwelling areas in 2013. In contrast, the high catch years of 2004 and 2009, associated with elevated *Chl-a*, coincide with early and/or prolonged seasonal blooms. These are induced by strong winds over the Benguela upwelling and Cold Ridge areas in 2004, and by intensified negative wind stress curl over the Benguela upwelling area in 2009. These results show that the squid catch fluctuations are potentially predictable and could support policymakers seeking to improve their planning of adaptation strategies and risk mitigation.

1. Introduction

Changes in phytoplankton productivity and coastal upwelling systems often affect the oceanic food web, including commercially valuable fish species and the coastal communities dependent on them. The occurrence of such changes and their repercussions are likely to become increasingly common with future climate change, especially in regions with multiple upwelling systems and rich fishing grounds, such as the South African coast (Bakun et al., 1998, 2015). This oceanic region, at the gateway between the Indian and Atlantic Oceans (Fig. 1a), is

uniquely puzzling with its heterogeneous and complex circulation dynamics, driven by different atmospheric and oceanographic forcing (e.g., Lutjeharms, 2007). The surface circulation in South African waters connects the Agulhas Current (AC), a western boundary current, to the Benguela Current (BC), an eastern boundary current (Matano, 2020; Veitch and Penven, 2017). The AC flows south-westward from 27°S to 40°S, with velocities reaching 2.5 m s⁻¹ (Beal and Bryden, 1999; Lutjeharms, 2006; Fig. 1a). The AC changes direction at its westernmost position, generally located at around 18–20°E and 39.5°S, where it retroflects back into the Indian Ocean as the Agulhas Return Current

* Corresponding author.

E-mail address: fatma.jebri@noc.ac.uk (F. Jebri).

<https://doi.org/10.1016/j.dsr2.2022.105028>

Received 28 May 2021; Received in revised form 11 January 2022; Accepted 15 January 2022

Available online 23 January 2022

0967-0645/© 2022 The Authors. Published by Elsevier Ltd. This is an open access article under the CC BY license (<http://creativecommons.org/licenses/by/4.0/>).

(ARC) (Dencausse et al., 2010; Russo et al., 2021; Fig. 1a). At the Agulhas retroflexion, rings, eddies, and filaments are released, influencing the flow of the BC. The AC flow can be divided into a northern stable part (north of $\sim 34^{\circ}\text{S}$) and a southern part (south of $\sim 34^{\circ}\text{S}$), which meanders (Paldor and Lutjeharms, 2009), shedding cyclonic eddies over the mid-shelf region and offshore edge of the Agulhas Bank (Penven et al., 2001). The southern AC is more unstable due to horizontal shear instability, leading to the formation of sub-mesoscale cyclonic eddies (Krug et al., 2017). Cyclonic eddies in the southern AC landward border, known as shear edge eddies, travel downstream and are most prevalent in the Agulhas Bank shelf bight (Lutjeharms et al., 2003). The strong effect of the AC on the Agulhas Bank also includes a Natal Pulse (which is a large meander that forms near the Natal Bight and travels southward), forcing the current onto the Bank (Jackson et al., 2012). Natal Pulses contribute to upwelling in the outer and inner shelf regions (Krug et al., 2014). The intensification of the AC jet associated with large meanders and its divergence from the coast can generate localized shelf edge upwelling, facilitating shelf-slope exchange (Lutjeharms et al., 1989; Lutjeharms, 2006; Leber et al., 2017; Malan et al., 2018). However, the larger scale upwelling takes place along the South African west coast (southern Benguela upwelling) and on the Agulhas Bank (Cold Ridge) during austral summer (October to April), when the intense northward and north-westward winds blow parallel to the southwest and south coasts (Boyd and Shillington, 1994; Schumann, 1999; Desbiolles et al., 2014; Strub et al., 2020; Jacobs et al., this issue) (Fig. 1b). The southern Benguela upwelling is usually observed between 26.5°S and 34°S and is characterized by the resurgence of cold and nutrient-rich water in the coastal fringe (Desbiolles et al., 2014; Fig. 1a). The Cold Ridge upwelling, known to be initiated by wind forcing and strengthened by westward advection, appears at the ocean surface or sub-surface as a colder filament with relatively fresher and more productive waters extending from the southeast edge of the Agulhas Bank and along the 100 m isobath (Boyd and Shillington 1994; Roberts, 2005; Jackson et al., 2012; Matano et al., 2020; Jacobs et al., this issue; Fig. 1a).

The productive South African waters help sustain rich ecosystems and fishing activities which play a major role in certain coastal fishing communities (Zantsi et al., 2013). Specifically, the squid fishery has been declared one of the most valuable fisheries in South Africa (Augustyn et al., 1994). It supports $\sim 25,000$ livelihoods (Cochrane et al., 2014) and provides employment opportunities for about 3000 people (DAFF, 2009) in a country suffering from very high unemployment rates (32% in 2020, according to Stats SA (2020)). This fishery contributes 9.3% to the total catch sales of the fishing sector (Zantsi, 2013). Squid fishery products are mostly (98%) exported to international markets such as Europe and Asia (DAFF, 2013; Zantsi, 2013). In South Africa, the squid fishery is mostly conducted by local fishing fleets along a substantial portion of the Agulhas Bank (Olyott et al., 2007) and along the west coast of South Africa (Augustyn, 1991), as squids are distributed between Namibia and the wild coast of the Eastern Cape ($\sim 29^{\circ}\text{E}$) (DEAT,

2005; DAFF, 2013; Lipiński et al., 2016). This fishery targets *Loligo reynaudii* which is the most abundant squid in the region. *L. reynaudii* is commonly called ‘chokka’ (Roberts and Sauer, 1994), and hereafter referred to as ‘squid’. The squid spawn in inshore waters, most commonly on the Agulhas Bank (e.g., Roberts and Van den Berg, 2002). Some squid paralarvae and juveniles are transported from the bank to feed and grow in the western nurseries within the more productive Benguela upwelling waters (Hutchings et al., 2002; Olyott et al., 2007), but, overall, the paralarvae distribution pattern is complex as they are found in different areas along the South African coast (Lipiński et al., 2016). Despite the fishing effort control measures implemented since the late 1980s (Zantsi et al., 2013; DAFF, 2013), the squid catch declined to extremely low levels in 2013, impacting many fishers’ income and employment (Joyner, 2015; Mthembu, 2019). Overexploitation and environmental controls have since been debated as potential causes of the squid fish stocks crash and production loss in 2013 (Joyner, 2015; Augustyn et al., 2017). Investigating changes in the marine environment can help understand potential environmental drivers of low catches and guide the level of response required in case of future similar situations. This is particularly important as the environmental conditions influence the squid life cycle and catches (e.g., Roberts, 2005; Jury, 2019). Moreover, changes in small pelagic fish species (anchovy and sardine), attributed to environmental factors, were observed off the south coast of Africa during 2013 (Augustyn et al., 2017), which further favours the hypothesis of environmental change affecting the pelagic species’ abundance. Although efforts towards a more sustainable management strategy of the squid resource have been on-going (Augustyn et al., 1992; Zantsi et al., 2013; Mwicigi et al., 2018), no studies have examined the influence of long-term environmental changes on the squid catches based on observations, and very few model-based investigations have attempted to address the squid catch declines. Based upon principal observations of satellite-derived ocean colour, ecological indicators such as phytoplankton abundance and phenology (timing of growth) can be derived, enabling a quantitative assessment of the status of marine ecosystems and their resources (e.g., fisheries) (Platt et al., 2003, 2009).

To this aim, advances in satellite remote sensing of ecological indicators can be an important aid in bridging the gap between ocean productivity and fish catch variations (e.g., Platt and Sathyendranath, 2008; Jury, 2011; Raitso et al., 2015; Kassi et al., 2018; Jury, 2019; Jebri et al., 2020; Gittings et al., 2021). This study is intended to advance knowledge of the linkages between squid catches and the biophysical controls as determined from long-term satellite-derived observations of South African coastal waters. Variations of the squid catch and chlorophyll-*a* (*Chl-a*, a proxy for phytoplankton biomass), one of the indicators of fish abundance (Chassot et al., 2011), are examined interannually with a focus on years of low and high catches. The response of seasonal phytoplankton blooms to ocean physics (Sea surface temperature (SST), surface currents, winds) is assessed over the region. Changes in *Chl-a* and physical regimes are identified, specifically

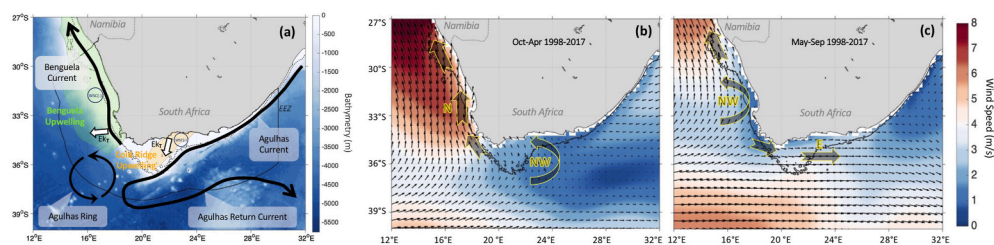


Fig. 1. (a) Bathymetry (in m) and schematic of the main surface currents, seasonal upwellings and associated wind drivers over the South African waters. The Agulhas Current (AC), the Agulhas Return Current (ARC) and the Benguela Current (BC) are illustrated with solid black arrows based on Beal et al., (2011). An AC ring is shown with a black circle. Approximate locations of the Benguela and Cold Ridge upwellings are illustrated with light green and light orange shaded areas, respectively. The white arrows

and blue circles represent Ekman transport (Ek_T) and WSC(–) respectively. The -Atlantic & Cape-part of the South African EEZ is delimited by the thin black contour. Wind speed and vectors (in m s^{-1}) are shown (b) during Oct–Apr 1998–2017, period of North (N) and North-westward (NW) winds and (c) during May–Sep 1998–2017 when the winds are North-westward (NW) and Eastward (E). Note that the long-term averaging Oct–Apr (May–Sep) wind patterns have a similar layout as the individual months Oct to Apr (May to Sep) 1998–2017. The 200m isobath derived from ETOPO21 global gridded database is represented by the dotted black line on panel (a) and by solid black line in panels (b) and (c).

during the catch decline/peak years, for which phytoplankton phenology metrics are also examined. Finally, the results are discussed in light of the current squid management practices and some perspectives are given regarding the predictability of the variations in abundance of this valuable resource.

2. Material & methods

2.1. Satellite ocean colour data

Monthly and 8-day satellite-derived *Chl-a* concentrations (mg/m^3) are obtained from the Ocean-Colour Climate-Change Initiative project (OC-CCI; version 4.2; Sathyendranath et al., 2020; <http://www.esa-oceancolour-cci.org/>), at a spatial resolution of 4 km. This dataset is the most consistent timeseries of multi-satellite (MODIS-Aqua, SeaWiFS, MERIS and VIIRS) global ocean colour data currently available (Racault et al., 2017). Although the monthly and 8-day composites of this *Chl-a* product span from September 1997 to December 2019, only the period extending until December 2017 is used here to match the time period of the available squid catch record (cf. section 3.1). The monthly *Chl-a* from 1998 to 2017 are used to examine the seasonal and interannual *Chl-a* variability over the study area. The 8-day *Chl-a* timeseries are exploited to derive the phenological indices of the seasonal phytoplankton bloom in the coastal zone.

Despite the multi-chlorophyll algorithm approach used in the OC-CCI processing (Jackson et al., 2017), satellite-derived *Chl-a* observations could still be overestimated in coastal shallow waters (generally shallower than 30m, Zhang et al., 2006). This limitation is due to the influence of suspended material and dissolved organic matter present in these optically complex waters which may result in high water leaving radiance, and in turn, an overestimation of the correction term (IOCCG., 2000). However, not all the high satellite *Chl-a* values in coastal regions are necessarily biases. They could reflect chlorophyll-rich detritus from a riverine source that enhances phytoplankton production near the coast or highly productive coral reef zones (Raitso et al., 2013, 2017). For example, the enhanced *Chl-a* values exceeding $2.5 \text{ mg}/\text{m}^3$ over a narrow band along South Africa's coastline (e.g., Supplementary Figs. 8a and b) could be explained by the presence of several riverine inputs (FAO., 2016). It has been shown that *Chl-a* nearshore signal could be associated with turbidity, and that Fluorescence Light Height, estimated from the red spectral band (and thus less sensitive to coastal sediments) may better represent productivity (Jury, 2019). However, the study area here comprises mainly Case-I open ocean waters.

2.2. Phytoplankton phenology metrics

We estimate the timing of bloom initiation and termination (i.e., the phytoplankton phenology metrics) based on the threshold criterion method (e.g., Racault et al., 2012) applied to the 8-day satellite *Chl-a* data from 1998 to 2017. The concept of the threshold criterion method focuses on the fact that a phytoplankton bloom occurrence corresponds to a significant increase in *Chl-a* above “normal” concentrations (Siegel et al., 2002). Note that this method requires a gap-free *Chl-a* timeseries as an input, thereby a linear least squares interpolation is applied to fill in missing data in the timeseries using the MATLAB subroutine *inpaint_nans* (D'Errico, 2012). Firstly, the acquired 8-day satellite *Chl-a* timeseries are spatially averaged over each of the three coastal areas of interest (A1-A3). These regions of interest retrieved from a point-by-point correlation of surface *Chl-a* anomalies with wind speed and WSC anomalies over the South African coast region during Oct–Apr 1998–2017 (cf. Fig. 4a and b and section 3.2). They consist of the coastal areas defined by the pixels that fall within the 0.3 contour (i.e., correlation coefficients higher than 0.3) of the significant correlations, at 95% level, between the *Chl-a* and wind speed (A1-3) and the *Chl-a* and WSC (B1-2), as approximately delimited by the thick blue contour lines in Fig. 4 (a) and (b). Secondly, a visual analysis of the *Chl-a* seasonal

climatology in each region is conducted to identify two separate time intervals in the calendar year, from which the phenology metrics are computed. These two main periods are defined for regions A2-3 (A1), as 1) January (February) to July, which covers the “autumn” period where phytoplankton biomass is shown to peak between March and May, and 2) August to December (January of year $t+1$) for the “spring” phytoplankton bloom which is shown to peak between September and November. Note that for area A1, the two-time intervals are altered slightly to account for the high *Chl-a* concentrations observed at the beginning of the year (e.g., Figs. 7 and 8a,d) which is most likely related to the continuation of the spring bloom of the previous year. Thirdly, we define the threshold criterion as the long-term median of the *Chl-a* timeseries for each season, plus 10%. This threshold is selected as it was found to be the most representative of the bloom initiation and termination metrics for each season over the twenty years of observations. Using this threshold, *Chl-a* anomalies are computed by subtracting the threshold criterion from the timeseries and the cumulative sums of anomalies are calculated. Increasing (decreasing) trends in the cumulative sums of anomalies represent periods when *Chl-a* concentrations are above (below) the threshold criterion. The derivative of the cumulative sums of anomalies is then used to identify the timing of the transition between increasing and decreasing trends. The initiation of the seasonal phytoplankton bloom corresponds to the 8-day period when *Chl-a* concentrations first rise above the threshold criterion (i.e., when the gradient of the timeseries first changes sign). The termination of the phytoplankton bloom is subsequently computed as the time when the derivative is equal to zero (after the timing of initiation). For each season, the climatological phenology metrics (e.g., grey solid lines in Figs. 7 and 8) in each region are calculated by computing the average of the annual metrics retrieved for each year.

Due to the study region's complex circulation dynamics which may be ephemeral and highly spatially heterogeneous in nature (cf. section 1), some seasons can be characterized by highly variable *Chl-a* concentrations. This makes the phenology algorithm prone to detecting multiple occasions where *Chl-a* concentrations rise above and below the threshold criterion. Subsequently, to stabilise the detection of the phenology metrics, two additional criteria are employed to define, more robustly, the conditions needed to recognise a phytoplankton bloom in the region. The first additional criterion is that *Chl-a* concentrations must remain above the threshold for ~ 3 weeks for a phytoplankton bloom to be identified (as proposed by Racault et al., 2015, where the authors used a period of 16 days). Similarly, if *Chl-a* concentrations fall below the threshold for < 3 weeks following the bloom initiation, it is not recognised as a bloom termination. The second criterion is that seasons with multiple phytoplankton blooms (as detected by the first criterion) are deemed as too heterogeneous for the retrieval of reliable phenology metrics and removed from the analysis. Thus, depending on the region/season, the phenology algorithm can robustly detect a clear seasonal phytoplankton increase period for a particular year. We note that the threshold methodology has been successfully utilised in different regions of the global oceans (Racault et al., 2012, 2015; Gittings et al., 2018, 2019) using various thresholds (5%, 10%, and 15%), depending on the type of analysis (e.g., interannual or climatological).

2.3. Wind, currents and SST data

The ERA-5 reanalysis 10 m zonal and meridional winds produced by the European Centre for Medium-Range Weather Forecasts (ECMWF) are used in the study. This dataset is obtained from the Climate Data Store (CDS) dataset (<https://cds.climate.copernicus.eu/cdsapp#!/dataset/reanalysis-era5-single-levels-monthly-means?tab=overview>; Hersbach et al., 2019) at a horizontal spatial resolution of 25 km as monthly averages from 1979 to present. We consider the period 1998–2017 to calculate the climatological means of wind fields to match the *Chl-a* data. The wind speed is used to provide information on the Ekman transport wind-driven upwelling. This type of wind-driven upwelling

involves coastal alongshore winds which bring nutrient-rich waters towards the surface. Note that Ekman transport is proportional to wind stress and hence to wind speed (cf. Eq (2) below).

We also examine the Wind Stress Curl (WSC) which is a sign of vertical pumping and proportional to the vertical velocity. Negative WSC (hereafter WSC(-)) in the southern hemisphere, as the case of the study area, indicates ocean surface divergence forcing waters upward (upwelling - Ekman suction) (Gill, 1982; Pickett and Paduan, 2003). In contrast, positive WSC implies convergence forcing waters downward (downwelling - Ekman pumping). The WSC is calculated by using the wind stress fields in the following equation:

$$WSC = \frac{\partial \tau_y}{\partial x} - \frac{\partial \tau_x}{\partial y} \quad (1)$$

where τ_x and τ_y are the zonal and meridional components of the wind stress and x and y are the zonal and meridional dimensions. The wind stress fields were computed using the Gill (1982) equation:

$$\tau = \rho_a C_d |\mathbf{v}| \mathbf{v} \quad (2)$$

Where τ and \mathbf{v} are the wind stress wind vectors, respectively. ρ_a is the air density (1.2 kg/m^3) and C_d is the drag coefficient equal to 0.0013 following Large and Pond (1981) for regions where winds at 10 m are generally weaker than 11 m s^{-1} (cf. Fig. 1a). Note that Eq. (2) approximates the wind stress as a function of the atmospheric winds alone and neglects ocean surface velocity. This component associated with the current effect is typically $0.2\text{--}0.3 \text{ m s}^{-1}$ which is very small (at least 10 to 26 times smaller) compared to the wind component which is typically at $3\text{--}8 \text{ m s}^{-1}$ over the South African shelf, and thus can be neglected (Supplementary Fig. 1). Additionally, the observed current-stress coupling coefficient between surface geostrophic currents and surface stress shows small values (0 to $-0.5 \cdot 10^{-2} \text{ N s m}^{-3}$) over the Agulhas Bank and the western South African shelf, which indicates a weak imprint of the current on the surface stress (Renault et al., 2017, their Fig. 2a).

We use the reprocessed Met Office Operational-Sea-Surface-Temperature-and-Sea-Ice-Analysis (OSTIA) SST product, acquired from the Copernicus Marine Environment Monitoring Service (CMEMS) (<http://marine.copernicus.eu/services-portfolio/access-to-products/>). This multi-satellite global SST dataset is provided daily at 5 km spatial resolution over the period 1981 to 2020. We compute monthly SST means to assess the long-term seasonal and interannual variations from 1998 to 2017 to be consistent with the remotely sensed *Chl-a* and squid catch datasets.

Another satellite product used here is the altimetry-derived absolute geostrophic currents processed by CLS (previously by AVISO (Archiving, Validation and Interpretation of Satellite Oceanographic Data)) and distributed by CMEMS (<http://marine.copernicus.eu/services-portfolio/access-to-products/>). These are daily geostrophic zonal and meridional velocities gridded at 25 km spatial resolution from the delayed time DUACS_DT2018 version and spanning the period

1993–2020. We compute the monthly means over the period 1998–2017 to match the satellite *Chl-a* and squid catch datasets. The satellite currents are used to provide insight on the influence of the currents on the *Chl-a* variations.

2.4. Cumulative sums of anomalies

The cumulative sums method is applied to the *Chl-a*, wind speed and WSC monthly anomalies (cf. section 3.3) to assess the interannual variability by highlighting major changes in the monthly data and reducing the high frequency noise in the timeseries (Manly and Mackenzie 2000; Briceno and Boyen, 2010). This statistical analysis allows the extraction of information on timeseries patterns and trends (here *Chl-a*) in relation to potential drivers (here winds) when applied to a number of variables (Regier et al., 2019). Note that the cumulative sums transformed timeseries are not appropriate for the application of linear regression, or any other statistical tests, because they increase the autocorrelation in a timeseries (Regier et al., 2019; Tilstone et al., 2015). For our analysis we used a variant of cumulative sums where original values are normalized to a mean of zero and unit standard deviation (z-scores) before computing the running sum (Taylor et al., 2002). Cumulative sums and normalized cumulative sums both produce similar results when plotted, but the advantage of using z-scores is the direct comparison of different variables regardless of their absolute values. Normalized cumulative sums segments with increasing slopes represent positive temporal trends (positive anomalies) while segments decreasing slopes highlight negative temporal trends (negative anomalies), and horizontal segments indicate average conditions (Briceno and Boyen, 2010). A bowl-shaped (dome-shaped) cumulative sum curve describes an overall increasing (declining) trend (Briceno and Boyen, 2010). The cumulative sums technique has increasingly been used to determine underlying features of environmental timeseries including long-term *Chl-a* at the interannual scale (McQuatters-Gollop et al., 2008; Raitos et al., 2014; Tilstone et al., 2015; Liuzzo et al., 2017; Gittings et al., 2018; Kizenga et al., 2021).

2.5. Squid catch records

We use squid landings in tonnes of wet weight per month over the period 1985 to 2017, emanating from the commercial jig fishery in South Africa and provided by the South African Department of Forestry, Fisheries and the Environment (DFFE). The DFFE squid annual catches are estimated by summing the monthly landings for each year over the full-time record (1985–2017) and compared to squid landings from the *Sea Around Us* initiative (<https://www.seaaroundus.org/>; Lam et al., 2015). The *Sea Around Us* (SAU) catches are recorded within the *-Atlantic & Cape-*part of the South African EEZ (Fig. 2a) in tonnes of wet weight per year between 1950 and 2016. When comparing the two datasets the common period 1985–2016 is used, but for further analysis (section 3) the DFFE data for 1998–2017 are used to match the *Chl-a* time series. SAU considers the catch officially “reported” to the Food and

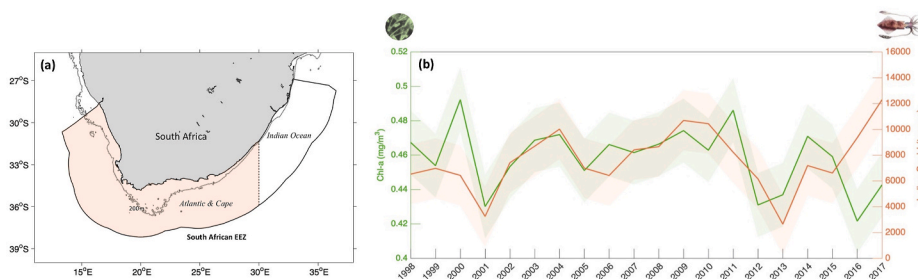


Fig. 2. (a) The squid fishing zone (light orange area) which corresponds to the Atlantic & Cape part of the South African EEZ (black contour). The 200m isobath derived from ETOPO2v1 global gridded database is represented by dotted black line. (b) *Chl-a* (mg/m^3) and squid catch (tonnes) annual variations from 1998 to 2017. The light shadings in panel (b) represent ± 2 standard deviation for both variables.

Agriculture Organization (FAO) or at the national level and estimates of “unreported” catch following the reconstructed catches method of Pauly and Zeller (2016). The comparison of squid landings by the DFFE and SAU over their common period 1985–2016 shows a high and significant correlation of $\Gamma = 0.91$ and a $P_{\text{value}} < 0.001$ (Supplementary Fig. 2). This relationship suggests that the interannual variability in the landings of squid observed in the South African fishing zone is representative of the landings for the -Atlantic & Cape-part of the South African EEZ. The fact that both sources of landings are consistent with each other and show similar patterns strengthens the trust in each of those datasets.

The squid landings data used here from both the DFFE and SAU are pure catches rather than catch per unit effort (CPUE). Landings have been exploited before to examine the link between environmental factors (e.g., temperature, *Chl-a*, phytoplankton phenology, etc.) and marine fish catch in coastal regions (Tzanatos et al., 2014; Kassi et al., 2018; Jebri et al., 2020). Although official landings do not necessarily represent stock abundance due to the absence of fishing effort impact, the FAO landing trends (such as those from *Sea Around Us*) are generally consistent with those of biomass from fully assessed stocks and demonstrate how catches have realistically changed over time (Froese et al., 2012; Pauly and Zeller, 2018). Additionally, to account for this potential bias, we compare DFFE CPUE data, existing as seasonal means for January to March from 1995 to 2017, to the corresponding seasonal landings (Supplementary Fig. 3). The seasonal landings show very similar patterns to the seasonal CPUE, the main difference being the magnitude rather than a change in the trend. This shows that landing trends indicate resource availability for this study’s region. Furthermore, the DFFE landings dataset is available for a longer time period and at higher frequency (monthly) than the seasonal CPUE, which is needed

for comparison with satellite *Chl-a* data and the phenology indices.

3. Results

3.1. Variability in squid catch and phytoplankton biomass

Annual squid catches over the -Atlantic & Cape-part of the South African EEZ, represented by the orange shaded area in Fig. 2a, are compared to corresponding satellite *Chl-a* from 1998 to 2017 (Fig. 2b). Both timeseries follow a similar pattern with a rise (fall) in squid catches associated, most of the time, with elevated (reduced) *Chl-a* concentrations. The highest significant correlation at the 95% level between the annual catches and *Chl-a* is found at 0-lag with a correlation coefficient of $\Gamma = 0.6$ and a P_{value} of 0.009 over the period 1998–2015 and $\Gamma = 0.4$ when data from 2016 to 2017 is included (see Discussion for details on the particularity of 2016–2017). Squid catches crashed to very low levels of ~3250 and ~2650 tonnes in 2001 and 2013, respectively which coincided with a decrease in phytoplankton biomass down to ~0.43 mg/m³ (Fig. 2b). In contrast, during other years with high catches (up to ~11,000 tonnes) such as in 2004 and 2009, the annual *Chl-a* levels increased to concentrations of ~0.47 mg/m³ (Fig. 2b). The specific years of low (2001, 2013) and high (2004, 2009) catches are further examined in terms of their *Chl-a* annual cycles relative to the climatological *Chl-a* and to corresponding catch annual cycles (Fig. 3).

The climatological *Chl-a* annual cycle over the South African squid fishing zone presents a bimodal pattern with two seasonal blooms – one in autumn (March–May) and the other in spring (September–November) (Fig. 3, green dashed line). During the spring bloom, *Chl-a* concentration peaks in October (0.53 mg/m³), whilst during the autumn bloom, the

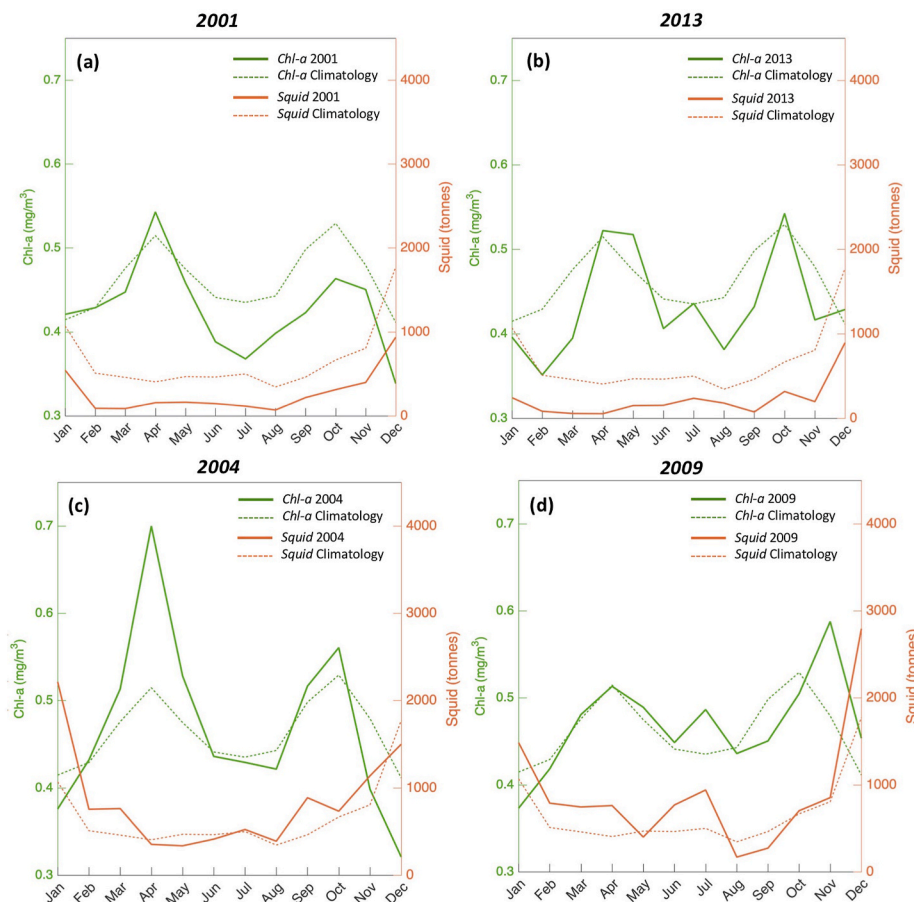


Fig. 3. Annual cycles of *Chl-a* (mg/m³) and catches (tonnes) during 2001, 2013, 2004, 2009 (solid lines) and their climatology (dashed lines) over the Atlantic & Cape part of the South African EEZ (black contour, Fig. 2a).

maximum concentration occurs in April (0.51 mg/m^3). These seasonal phytoplankton blooms are important to fishery abundance along the Agulhas Bank and the South African west coast (Shannon et al., 1984; Hutchings, 1994; Jury, 2019), and their timing matches the squid spawning periods (cf. Discussion).

The *Chl-a* annual cycle in 2001 shows lower values from May to December compared to the climatology (Fig. 3a). For example, the 2001 spring bloom peaked at 0.45 mg/m^3 while the *Chl-a* maximum in a normal spring is 0.53 mg/m^3 . Despite a small *Chl-a* increase in April, the autumn bloom of 2001 was anomalously low compared to the climatological *Chl-a*, with lower values in autumn (Fig. 3a). In parallel to the overall decrease of *Chl-a* in 2001, the catches did not exceed 1000 tonnes during the same year, which is substantially reduced compared to a normal year (Fig. 3a). Although the phytoplankton biomass reached normal levels in April and October 2013, the *Chl-a* annual cycle in 2013 reveals very low concentrations during the initiation and termination of the spring bloom, and low *Chl-a* concentrations at the commencement of the autumn bloom compared to the climatology (Fig. 3b) (see more details on bloom phenology in section 3.4). The squid catches in 2013 are under 500 tonnes all year, except in December when they reached ~900 tonnes, which still remains anomalously low compared to the ~1800 tonnes usually caught at the end of a normal year (Fig. 3b).

In 2004 – a year of generally higher catches than the climatological mean – *Chl-a* values increased considerably in autumn, reaching 0.7 mg/m^3 in April which is 34.6% of the climatological level (Fig. 3c). *Chl-a* concentrations in spring 2004 were also higher than normal between September and October, with values up to 0.57 mg/m^3 (Fig. 3c). During 2009, *Chl-a* conditions were normal in autumn and the spring bloom shifted by one month, with a later start in October (Fig. 3d). However, elevated *Chl-a* concentrations (0.5 mg/m^3) are seen at the start of the bloom (October), followed by a maximum (0.59 mg/m^3) in November which is about 12.16% higher than the normal spring bloom peak and 31.11% higher than a normal November (Fig. 3d). Additionally, a third *Chl-a* small peak (0.48 mg/m^3) is observed in July 2009. The enhanced phytoplankton biomass in 2009 is, overall, coherent with the squid catches which are larger than those in 2001 or 2013, and generally higher than normal (Fig. 3d).

3.2. Physical control on phytoplankton abundance

In this section, potential physical mechanisms determining phytoplankton abundance over the squid fishing zone are examined. Spatial

correlations between *Chl-a* anomalies and selected physical variables (wind, WSC, SST and surface currents) are calculated on a pixel-by-pixel basis over the South African waters for the period October–April in each year from 1998 to 2017 (Fig. 4). Note that the same maps for the period May–September 1998–2017 show generally weak or insignificant correlations in the coastal areas (Supplementary Fig. 4 and Text 1). In contrast to the May–September period, October–April (Oct–Apr hereafter) is a time when winds are directed northward along the west South African coast and north-westward along the central Agulhas Bank (Fig. 1b and c) which are favourable configurations for Ekman transport upwelling (and hence high productivity due to the upwelling of nutrients). Additionally, seasonal blooms occur within the South African EEZ during Oct–Apr (cf. Fig. 3 and section 3.1).

The analysis of the *Chl-a* versus wind speed and WSC provides insight into the influence of wind driven mechanisms. *Chl-a* and wind speed anomalies show positive and significant correlations (up to 0.6 with $P_{\text{value}} < 0.05$) along three main coastal regions (A1–A3, as highlighted by the blue contours on Fig. 4a; see section 2.2 for details), suggesting the occurrence of coastal wind-driven upwelling or enhanced vertical mixing. Vertical mixing was considered insubstantial during this period (Jacobs et al., this issue) whereas coastal wind-driven upwelling (e.g., Risien and Chelton, 2008) has been confirmed along those areas that correspond to the locations of the Benguela (areas A1, A2) and Cold Ridge (area A3) upwellings (Roberts, 2005; Junker et al., 2015; Jacobs et al., this issue). *Chl-a* and WSC anomalies during Oct–Apr reveal negative correlations (down to -0.6 with $P_{\text{value}} < 0.05$) over two main regions within the South African EEZ which can be linked to the Benguela and Cold Ridge upwelling zones (see blue contours on Fig. 4b, areas B1 and B2; see section 2.2 for details). This *Chl-a* and WSC relationship indicates the presence of another type of wind-driven upwelling due to Ekman suction (Gill, 1982; Pickett and Paduan, 2003). This process, commonly known as open ocean upwelling, is activated when $\text{WSC}(-)$ generates ocean-surface divergence, forcing water upward (e.g., Leber et al., 2017 and references therein).

Surface current speed is compared with *Chl-a* to examine the influence of currents on *Chl-a* spatial variations. *Chl-a* anomalies are negatively correlated (up to -0.5 with $P_{\text{value}} < 0.05$) with surface current speed anomalies at the outer edge of the eastern Agulhas Bank (from 23°E to 28°E , Fig. 4c) which corresponds to the AC's main location (Fig. 1a). This anti-correlation suggests that weak (strong) currents lead to high (low) *Chl-a*. In fact, as the meanders propagate along the AC, it is possible that they reduce its speed, move it offshore and induce

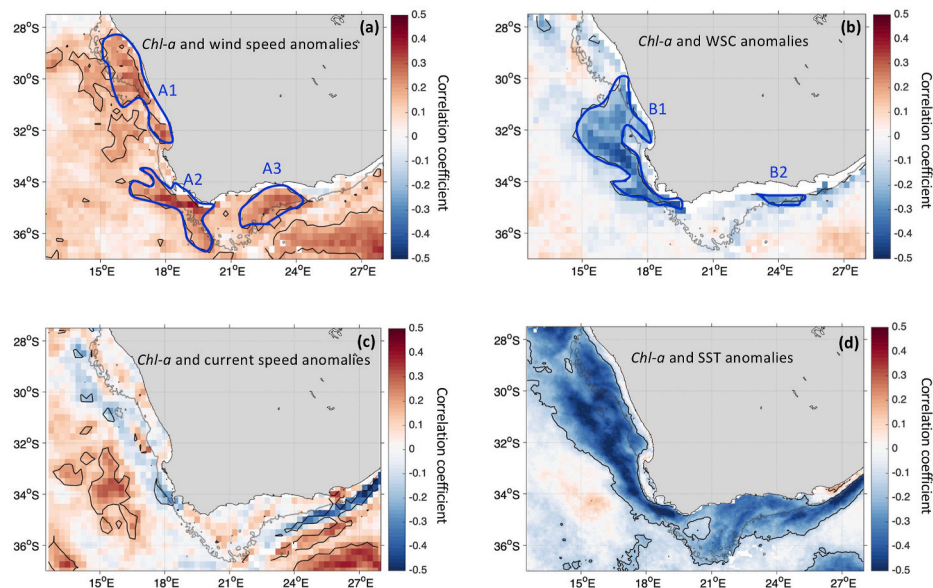


Fig. 4. Spatial correlations of satellite *Chl-a* with (a) wind speed, (b) WSC, (c) current speed and (d) SST anomalies off the South African coast during Oct–Apr 1998–2017. The 200m isobath derived from ETOPO2v1 global gridded database is represented by the grey dashed line. Significant correlations values at the 95% level (i.e., with $P_{\text{value}} < 0.05$) are highlighted by the black contours. The thick blue contour lines on panels (a) and (b) represent the coastal area with significant and high correlations between *Chl-a* and wind speed (A1–3) and between *Chl-a* and WSC (B1–2).

upwelling of cooler and nutrient-rich waters (e.g., Leber et al., 2017 for the AC region around 34°S), leading to phytoplankton growth. Note that this current-*Chl-a* relationship appears in Fig. 4c as a band because the meanders propagate along the AC path. It is also important to note that meanders and Natal pulses influence overall the interaction of the southern AC with the shelf circulation, driving upwelling/downwelling events across the inshore front of the current and on the shelf slope, in turn affecting nutrient supply (Krug et al., 2014; Malan et al., 2018). Although correlations between surface currents and *Chl-a* are weak on the central Agulhas Bank (i.e., along the Cold Ridge, cf. Fig. 1a) during Oct–Apr (Fig. 4c), they are strong and significant during December–February over the Cold Ridge (Supplementary Figs. 5a and b). This suggests that at this time of the year the currents may have an advective effect, acting along with the winds to bring nutrients and contributing to elevated *Chl-a* levels along the Cold Ridge pathway. Such an advection mechanism is consistent with previous analysis using in-situ and modelling data (Roberts, 2005; Jacobs et al., this issue).

The SST-*Chl-a* relationship is explored to provide information on the presence of cooler waters, which may indicate an enhanced nutrient supply and elevated phytoplankton biomass. Significant negative correlations (up to -0.7 with $P_{\text{value}} < 0.05$) are observed between *Chl-a* and

SST anomalies over most of the Agulhas Bank and the South African west coast (Fig. 4d). This is particularly marked in areas where phytoplankton blooms occur, such as the Cold Ridge and Benguela upwellings (Fig. 1a). These upwelling areas, based on the wind and *Chl-a* analysis (Fig. 4a and b), can bring nutrients to the surface. Additionally, SST and *Chl-a* exhibit a strong negative correlation along the southeastern side of the Agulhas Bank (Fig. 4d) where the AC mainly flows (Fig. 1a). The negative SST-*Chl-a* correlation on the outer edge of the eastern Agulhas Bank shows that high (low) *Chl-a* is related to cold (warm) waters. This result further strengthens the finding of the negative correlation between *Chl-a* and currents, suggesting that upwelling of cool and nutrient-rich waters can possibly be induced as the AC moves offshore (e.g., Leber et al., 2017, for the AC part around 34°S).

Noteworthy are the strong positive and significant correlations detected further offshore in the path of the ARC and its associated meanders (20°E to 28°E and south of -36°N); between *Chl-a* and wind speed; *Chl-a* and surface currents, and *Chl-a* and SST. The area centered around 27°E and 36°S is where *Chl-a* is strongly correlated with wind speed, current speed and SST. As this is a region where eddy activity and meanders can occur (e.g., Elipot and Beal, 2015; Penven et al., 2001; Lutjeharms et al., 2003; Paldor and Lutjeharms, 2009; Krug et al., 2017;

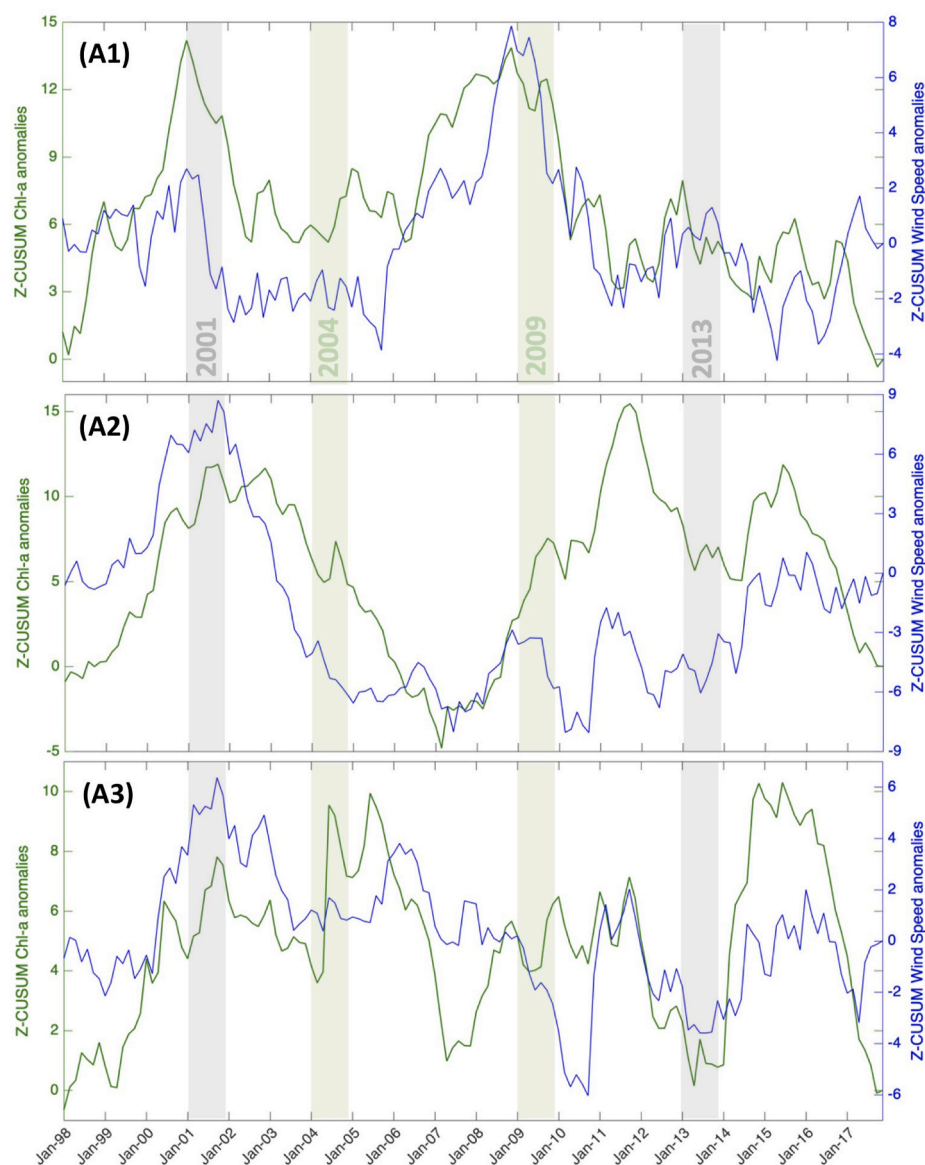


Fig. 5. Cumulative sums of monthly *Chl-a* and wind speed anomalies during Oct–Apr 1998–2017 over Benguela upwelling (A1, A2) and the Cold Ridge (A3) areas. The Cumulative sums summarizes major changes by smoothing high frequency noise along the time-series (see section 2.4 for more details). Increasing slopes represent positive temporal trends (periods with above average values) while decreasing slopes highlight negative temporal trends (periods with below average values), and horizontal segments indicate average conditions.

Malan et al., 2018), vertical mixing is likely at play.

Collectively, the spatial correlations suggest that what drives the *Chl-a* response near the coasts during Oct–Apr is dependent mainly on local wind forcing. They indicate the occurrence of two wind-driven upwellings via Ekman transport (coastal wind-driven upwelling) and Ekman suction (open ocean upwelling) over the South African west coast (Benguela upwelling) and the central Agulhas Bank (Cold Ridge). The surface currents appear to be more important for shelf edge processes and advection along the central Agulhas Bank on shorter time scales.

3.3. Wind-induced upwelling during catch's decline/peak years and low *Chl-a* regimes

Here, we investigate changes in the wind forcing during the squid catch declines (2001, 2013) and what characterized the wind conditions during the high catch years (2004, 2009) relative to changes in *Chl-a*. For this, cumulative sums are applied to monthly anomalies of *Chl-a*, wind speed and WSC during Oct–Apr 1998–2017, over the Benguela and Cold Ridge upwellings (for their position see Fig. 4; blue contour lines) (Figs. 5 and 6). The cumulative sums are an efficient statistical method that allows objective detection of changes in slope/trends in datasets, shifts and quantification of the driver-response relationship between variables (e.g., Regier et al., 2019) (see section 2.4 for more details). The cumulative sums method was applied as the untransformed data (i.e., monthly timeseries) provided little information (see Supplementary Figs. 6 and 7, and Text 2) on the relationships between the variables (*Chl-a*, wind speed and WSC) for specific years or changing trends. The focus was to determine the biophysical conditions (*Chl-a* and wind) associated with the extreme (anomalous) catch events (2001, 2004, 2009 and 2013).

The cumulative sums of *Chl-a* and wind speed anomalies show

similar patterns with generalized declines and increases in *Chl-a* mirrored in wind speed variations for the three areas A1, A2 and A3 (Fig. 5). This common feature of all zones reaffirms, to a large degree, the overall influence of the winds on *Chl-a*. Important shifts in terms of phytoplankton abundance are clearest for area A2, with pronounced *Chl-a* decreases during 2001–2006, 2012 to 2014 and mid-2015 to 2017. Area A1 reveals a more variable *Chl-a* pattern with small declines (in 2005–2006; 2013–2014; 2016–2017) in addition to large shifts (from 2001 to late 2003, and from late 2008 to 2011). In area A3, low *Chl-a* phases are more difficult to define (with a fluctuating signal despite the cumulative sums smoothing) but appear to start from late 2001 until 2003, succeeding the first decline in the other regions. Stronger *Chl-a* declines are then observed from mid-2005 to mid-2007, late 2011 to 2013 and mid-2015 to 2017. Those low *Chl-a* regimes in the three areas (A1–3) are largely coherent with wind speed reduction.

Low phytoplankton biomass during the catch decline years can be observed over one coastal area or collectively (Fig. 5). In 2001, a substantial decreasing phase in *Chl-a* and wind speed (negative slopes) began over area A1 and continued until approximately mid-2003 (Fig. 5, A1). A below average *Chl-a* and wind speed period (steep negative slopes) is seen during 2013 over areas A1 and A3 (Fig. 5, A1, A3). There is also a *Chl-a* decrease in 2013 over area A2 (negative slope) which is not well reflected in the wind intensity (Fig. 5, A2), but is likely due to the relaxed WSC as detected from B1 patterns (see Fig. 6, B1). High phytoplankton productivity characterized the high catch years 2004 and 2009 over the areas of interest. An increase in *Chl-a* (positive slope) associated with slightly above average winds occurred in 2004 over areas A1 and A3 (Fig. 5, A1, A3). In 2009, the cumulative sums charts for the areas A2 and A3 display elevated phytoplankton biomass (positive slope) but are not reflected in the wind intensity. The *Chl-a* increase over A2 in 2009 can be explained by the WSC(–) intensification as revealed by B1 cumulative sums (see Fig. 6, B1), while that of A3 is potentially

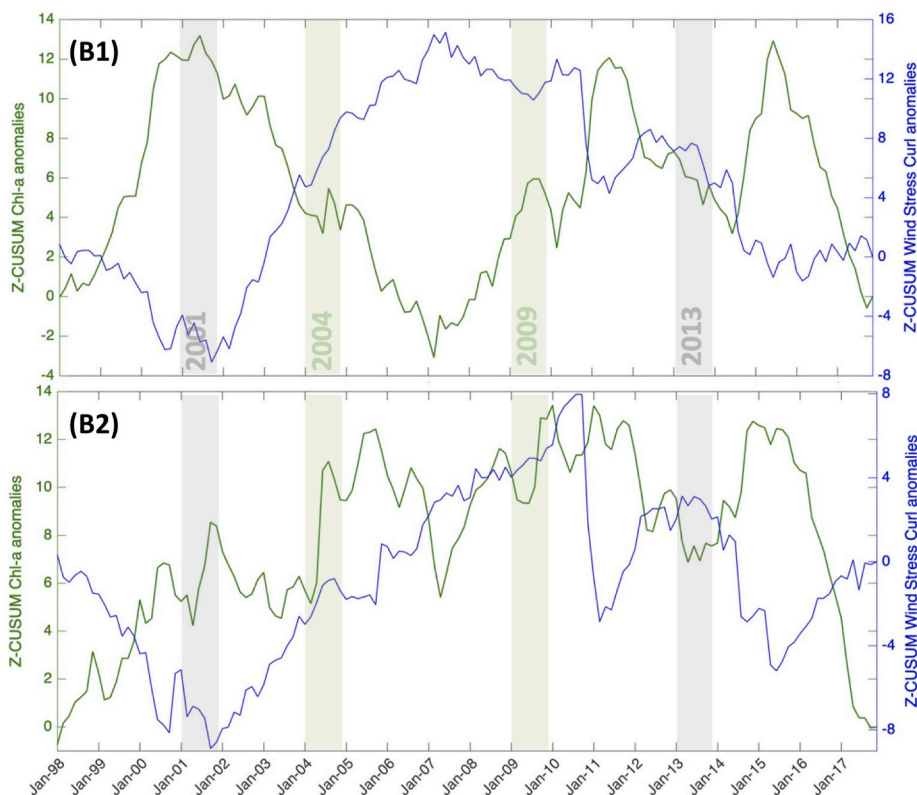


Fig. 6. Cumulative sums of monthly *Chl-a* and WSC anomalies during Oct–Apr 1998–2017 over Benguela upwelling (B1) and Cold Ridge (B2) areas. The Cumulative sums summarizes major changes by smoothing high frequency noise along the time-series (see section 2.4 for more details). Increasing slopes represent positive temporal trends while decreasing slopes highlight negative temporal trends, and horizontal segments indicate average conditions.

caused by other factors like advection (see section 3.2). In contrast to areas A2 and A3, the cumulative sums of *Chl-a* and wind speed over area A1 display a general decline (steep negative slopes) during 2009 which continued until 2011 (Fig. 5, A1).

The cumulative sums of *Chl-a* and WSC anomalies show both variables generally oscillating in anti-phase over areas B1 and B2 which demonstrates their close link (Fig. 6). Regime shifts regarding low *Chl-a* concentrations are apparent over area B1 during 2001–2007; 2012 to 2014, and mid-2015 to 2017. The *Chl-a* pattern over area B2 displays more frequent but shorter decreasing *Chl-a* phases from 2002 to 2004; 2006 to mid-2007; late 2011 to early 2011; late 2012–2013, and mid-2015 to 2017. The *Chl-a* negative slopes of both areas B1 and B2 are generally coincident with opposite trends in WSC, except for the period 2002–2008 in B2 where the WSC shows a steep positive slope while *Chl-a* oscillates between highs and lows.

Low phytoplankton productivity, as derived from the *Chl-a* – WSC relationship during the low catch years, is detected in the *Chl-a* decline (negative slope) over B1 from mid-2001, but is only reflected in the WSC (–) in late 2001 as it shifts towards above-average values (Fig. 6, B1). In 2013, decreasing *Chl-a* (negative slope) associated with relaxed WSC(–) (positive slope) occurred over areas B1 and B2 (Fig. 6, B1, B2). During the high catch year 2004, increasing *Chl-a* is seen over B2 (Fig. 6, B2). Although this enhanced *Chl-a* is not reflected in the WSC curve (positive slope indicative of WSC(–) relaxation), it is likely due to the stronger winds as deduced from the A3 cumulative sum chart (see Fig. 5, A3). The high catch year 2009 coincides with a *Chl-a* increasing period over both areas B1 and B2, which is associated with intensified WSC(–) (negative slope) over area B1 and is probably due to the presence of other factors over area B2 (Fig. 6, B1, B2).

In summary, the *Chl-a* declines in 2001 and 2013 occur amid or at the start of a low phytoplankton biomass regime. They are driven by weak winds and relaxed WSC(–) over the Benguela upwelling zone (A1, B1) in 2001, and over both Benguela and Cold Ridge upwelling zones (A1, A3, B1, B2) in 2013. Enhanced *Chl-a* is induced by strong winds over the Benguela and Cold Ridge upwelling areas (A1, A3) in 2004, and by

intensified WSC(–) over Benguela upwelling area (B1) in 2009. These findings further confirm that both wind-driven upwelling mechanisms (Ekman transport and Ekman suction) are at play, contributing to phytoplankton growth over both Benguela and Cold Ridge areas. Additionally, other drivers, such as advection, can cause *Chl-a* to increase over the Cold Ridge (areas B2, A3), as in 2009. The latter event could also be associated with the passage of Natal Pulses which can promote the uplift of the isotherms on the shelf region and maintain the Cold Ridge (Krug et al., 2014). A shelf-edge upwelling along the southeastern edge of the Agulhas Bank is also thought to be a source of the Cold Ridge (Jackson et al., 2012).

3.4. Phytoplankton phenology during catch's decline/peak years

Here, changes in bloom timing (phenology), considered important for fish stocks and larvae survival (e.g., Platt et al., 2003), are investigated. The phenology of the seasonal blooms during squid catch declines (2001, 2013) and peaks (2004, 2009) is explored based on their *Chl-a* timeseries and the corresponding timings of bloom initiation and termination (blue and orange lines, Figs. 7 and 8) over the productive areas, A1-3, defined from the *Chl-a* – wind analysis (cf. Fig. 4a). The climatological *Chl-a* and timings of bloom initiation and termination are also highlighted (black and grey vertical lines, Figs. 7 and 8). Details on the calculation of the phenology algorithm can be found in section 2.2.

In normal conditions, *Chl-a* increases in autumn and spring (black line timeseries) with spring (~September to November) blooms being shorter than autumn (~March to May) blooms (grey vertical dashed lines) over all areas except for area A1 where they show the same duration (see Figs. 7 and 8; Table 1, and Supplementary Text 3 for further details). The comparison of bloom phenology metrics for the years of interest (2001, 2013, 2004, 2009) to those determined for the climatology allows shifts in bloom initiation or termination during high/low catch years to be detected (Figs. 7 and 8, orange, dark blue and grey vertical lines).

Significant shifts in bloom phenology are detected in 2013 over the

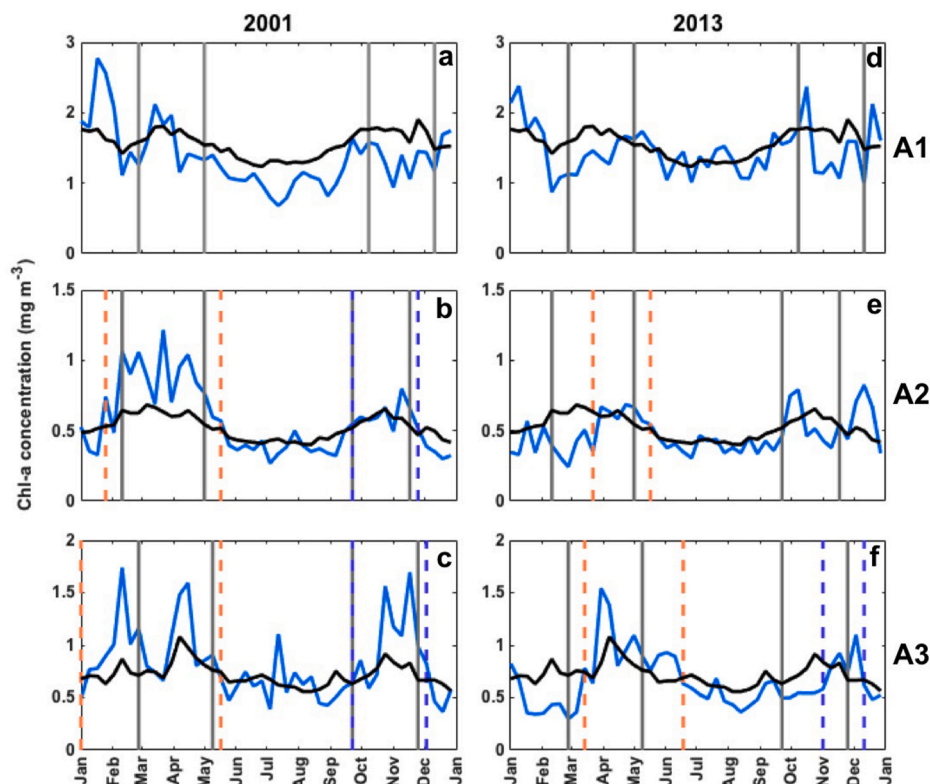


Fig. 7. Phenology metrics during (a–c) 2001 and (d–f) 2013 over Benguela upwelling (A1, A2) and Cold Ridge upwelling (A3) areas. The light blue lines represent the *Chl-a* annual cycle of specific year relative to the climatology (black lines) of the period 1998–2017 for each area. The climatological bloom timing (phenology) of initiation and termination are illustrated with the grey vertical lines. The timing of initiation and termination of the spring (autumn) bloom are shown with dark blue (orange) vertical dashed lines.

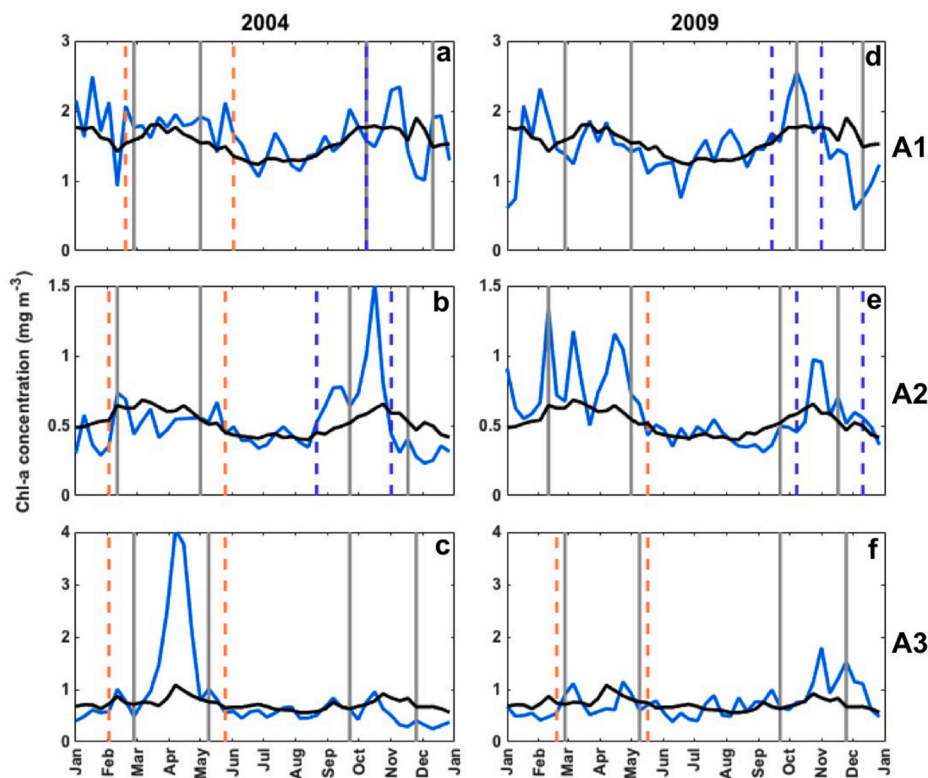


Fig. 8. Same as Fig. 7 but for 2004 and 2009.

Table 1

Climatological phenology indices (in days) in the three South African coastal regions A1-3 (see location in Fig. 4a) for autumn and spring phytoplankton blooms.

Area	Indices Autumn			Indices Spring		
	Initiation	Termination	Duration (days)	Initiation	Termination	Duration (days)
A1	26 Feb - 5 Mar	1-8 May	72	8-15 Oct	11-18 Dec	72
A2	10-18 Feb	1-8 May	88	22-29 Sep	17-24 Nov	64
A3	26 Feb - 5 Mar	9-16 May	80	22-29 Sep	25 Nov - 2 Dec	72

Benguela and Cold Ridge upwelling areas (A1-3). Over area A1, both the autumn and spring blooms are absent due to reduced *Chl-a* levels, with a maximum of 1.4 mg/m³ (excluding the spike of 2.2 mg/m³ in early October) instead of 1.8 mg/m³ in normal conditions (Fig. 7d). Over area A2, the autumn bloom is delayed (by ~1.5 months), with reduced *Chl-a* levels (~0.25 mg/m³) observed until the bloom initiation in mid-March (Fig. 7e). The autumn bloom in A2 is also shorter than the normal bloom duration by ~2 weeks (Table 1). A short *Chl-a* spike of 0.75 mg/m³ occurs in early October, followed by a decrease in *Chl-a* concentration for the remainder of the normal spring bloom period in A2 (Fig. 7e). A short, secondary peak (~0.8 mg/m³) also occurs in December. A delayed autumn bloom and shorter spring bloom, characterized by a late initiation (~1 month delay), occurred over area A3 as *Chl-a* concentrations remain lower than the climatology throughout the normal phytoplankton growth period (Fig. 7f). Note that the spikes in *Chl-a* by early October 2013 over areas A1-2 (Fig. 7d and e) are not substantially long to meet the bloom criteria, as *Chl-a* concentrations did not remain above the threshold for more than three weeks (see section 2.2 for more details).

Similar to 2013, phytoplankton phenology in 2001 appears unfavourable for productive conditions over area A1, with no autumn or spring bloom detected (Fig. 7a). Although a short *Chl-a* increase (of ~2 weeks) occurred over area A1 in autumn 2001, it did not constitute a bloom based on the three-week criteria (see section 2.2 for more details). In contrast, the bloom phenology over A2 and A3 is indicative of normal to higher productivity (Fig. 7b and c). In fact, the autumn blooms of

areas A2-3 show an earlier initiation and prolonged duration, while their spring blooms are characterized by a normal initiation and slightly longer duration (Fig. 7b and c).

During 2004, prolonged blooms are generally observed in each region (Fig. 8a, c). A longer and earlier autumn bloom is seen over area A1, whilst the spring bloom is characterized by a normal initiation and a substantially longer duration, ending in January of the following year (hence the bloom termination is not shown on the plot) (Fig. 8a). Area A2 displays earlier and longer autumn and spring blooms. During spring, a prominent *Chl-a* peak (1.5 mg/m³) occurs in mid-October which is not observed in any of the other years (Fig. 8b). Although no spring bloom is seen over the Cold Ridge area (A3), it presents an early and prolonged autumn bloom, with *Chl-a* reaching its absolute maximum (>3 mg/m³) in mid-April over twenty years of observations (Fig. 8c).

The bloom phenology metrics in 2009 suggest enhanced productivity over the three areas (A1-3; Fig. 8d, f). Area A1's spring bloom initiates ~1-month earlier, driven by a considerable *Chl-a* increase (reaching 2.5 mg/m³) in October, with a slightly shorter duration (Fig. 8d). However, no autumn bloom is detected over area A1 in 2009 (Fig. 8d). Over area A2, the *Chl-a* peaks in early February (~1.4 mg/m³), March and April (~1.2 mg/m³), induced a strong and prolonged autumn bloom which initiated unusually early in December of the previous year (hence the initiation is not shown on the plot) (Fig. 8e). The spring bloom of area A2 is longer but initiates slightly later than the climatology as the *Chl-a* main peak occurs in early November (~1 mg/m³) (Fig. 8e). Area A3 experienced a prolonged and earlier autumn bloom with distinct *Chl-a*

peaks ($\sim 1.1 \text{ mg/m}^3$) occurring in early March and late April (Fig. 8f). Although a spring bloom can be seen over area A3, with a *Chl-a* increase to $>1.5 \text{ mg/m}^3$ in November (Fig. 8f), the phenology algorithm did not detect a bloom initiation as *Chl-a* concentrations remained above the threshold at the beginning of the season (see section 2.2 for more details).

Overall, the phytoplankton phenology conditions during the low catch years (2013 and 2001) suggest absent, or short and delayed seasonal blooms over the Benguela upwelling area (A1) in 2001 and over both the Benguela and Cold Ridge upwelling areas (A1-3) in 2013. These phytoplankton phenology conditions are consistent with low phytoplankton productivity inferred from the *Chl-a* and wind regimes (cf. section 3.3) which affected all areas in 2013 and area A1 in 2001. The high catches of 2004 generally coincide with early and prolonged blooms over the Benguela and Cold Ridge upwelling zones (A1, A2 and A3 in autumn). The phytoplankton phenology in 2004 is, overall, coherent with *Chl-a* and the wind regime in A1 and A3 (cf. section 3.3). However, the early and longer A2 seasonal blooms in 2004 are not well reflected in wind conditions so are likely driven by other factors. The phenology metrics of the high catch year 2009 are largely in agreement with the *Chl-a* and wind regime over the Benguela upwelling area (A1). The early and/or prolonged seasonal blooms in 2009 over areas A2-3 are not well represented in the wind regime and thus are likely induced by other factors.

4. Discussion

The current study shows the importance of food availability for the chokka squid that have a short life span of about 12 months (Lipiński et al., 2020), explaining, to some extent, the long-term (twenty year) correlation found between squid catch and phytoplankton biomass (Fig. 2b). Interestingly, the highest significant correlation between these two variables is at no lag (Fig. 2b). The 0-lag significant correlation suggests that the changes (i.e., declines or increases) in phytoplankton availability and the caught squid occurs within the same year, but higher resolution data analysis is necessary to establish a more complete link (i.e., at smaller time scales). This 0-lag relationship is coherent with the age (less than one year old) of spawning squid aggregations (Lipiński et al., 2020 and references therein) which are targeted by the fishing industry (Downey et al., 2010; Lipiński, 1994; Sauer et al., 2013). It also suggests that low *Chl-a* or available at the wrong time of the year can have negative consequences on the adult squid (e.g., migrate elsewhere, do not form spawning aggregations). Note that a statistical significance of *Chl-a* and squid catch does not necessarily imply ecological causality. However, as phytoplankton forms the base of the marine food web, less *Chl-a* (Fig. 3) may lead to lower concentrations of zooplankton, the main food source for squid paralarvae (Augustyn et al., 1992; Olyott et al., 2007), and, in turn, less food for small fish and mid trophic level species like squid. Additionally, *Chl-a* available at the wrong time within the year (Figs. 7 and 8) may also impact paralarvae (Platt et al., 2003). For example, an early and/or longer bloom may lead to an increase in larval survival as a result of an increase in food availability. By contrast, a late bloom will likely lead to starvation (Platt et al., 2003).

Our results demonstrate that squid catch extremes may be linked not only to phytoplankton abundance but also to the timing of the bloom (Figs. 7 and 8), in agreement with the importance of these two indicators for larval survival (Platt et al., 2003). Reductions in larval survival and recruitment success can be induced by delayed or shorter-than-normal blooms, while spawning occurs at the original bloom timing (Cole, 2014). Spawning of squid takes place predominantly along the south coast and throughout most months of the year (Lipiński et al., 2016), with spawning at individual locations lasting weeks to months (Sauer and Lipinski, 1991). There are, however, generally two peak periods, one in spring/early summer (September–November/December) and another in autumn/winter (March–June/July) (Augustyn, 1990; Augustyn et al., 1994; Oosthuizen et al., 2002). October–December is

the period of maximum spawning intensity (Sauer et al., 1992; Olyott et al., 2006; Downey et al., 2010) and the most effective for sustaining the resource (Augustyn et al., 1994; Lipiński et al., 2020). A late bloom initiation and fewer plankton in the latter stages of the spawning seasons, such as in 2013 (Figs. 7 and 8), may decrease the chances of larvae surviving, thereby reducing recruitment and the total catch (e.g., Gittings et al., 2021). An opposite situation would be expected with an early and/or longer bloom (e.g., high *Chl-a* abundance and catches in 2004).

The squid resource is managed through effort control, including a five-week closed season (from 19 October to 23 November), allowing squid to spawn without fishing disturbance (e.g., Roel and Butterworth, 2000), while also reducing fishing effort (DAFF., 2013). Following the catch abrupt decline of 2013 and its drastic socio-economic consequences, an additional three-month (April to June) closed season was implemented from 2015 onwards (Mwiciigi et al., 2018). This measure likely led to the high catches of 2016 and 2017, despite their low annual *Chl-a* levels (Fig. 3), as the additional closed periods (from April to June in 2014, 2016 and 2017, and March to May in 2015) gave further time for the squid to recover after the 2013 crash. This notable change in fisheries regulations seems to have impacted the environment-squid relationship seen in earlier years (1998–2015). Additional years are needed to fully elucidate the consequences of the additional closed season on the catch and food availability link. Importantly, both October–November and April–June closures are coincident with the largest *Chl-a* seasonal peaks (Figs. 3 and 7) and spawning periods (Augustyn et al., 1994; Oosthuizen et al., 2002) which further adds support to the importance of the spring and autumn blooms for squid spawning and paralarval survival. This is also in line with the reported importance of the seasonal *Chl-a* blooms to the overall fish abundance in the region (Shannon et al., 1984; Hutchings, 1994; Jury, 2019). As with many short-lived species, biomass may be driven by environmental control (e.g., food availability and physical regime) (Zantsi et al., 2013).

Phytoplankton can become limited by the availability of nutrients when light and temperature are adequate and loss rates are not excessive (Hecky and Kilham, 1988). From May to September, *Chl-a* concentrations are low (Fig. 3) and physical controls are suggestive of weaker productivity (Supplementary Fig. 4). However, at this time the SST is coolest (Supplementary Fig. 8) and nutrient levels are highest (Jacobs et al., this issue) off the South African coast. Since May–September is not the upwelling season, the cooling and elevated nutrients are likely induced by the enhanced deep mixing, as shown by Jacobs et al., (this issue; their Fig. 4 and S2), for the Agulhas Bank. The enhanced mixing brings up nutrients and cool waters to the surface, but there is not enough light (cf., Mazwane et al., this issue; their Fig. 7b for the Agulhas Bank), and in turn the phytoplankton will not prosper in a similar scenario to the North Atlantic in winter (e.g., Martinez et al., 2011). During the productive summer period (Oct–Apr), *Chl-a* is highest (Fig. 3); SST is relatively cold at certain spots linked to upwelling (Fig. 4, Supplementary Fig. 8), and light is available (Mazwane et al., this issue; their Fig. 7b). However, the nutrients are not elevated (Jacobs et al., this issue) which suggests that nutrients are being directly consumed. Also, increased thermal stratification (stability) during the summer can result in phytoplankton being confined nearer the surface where there is more available light but nutrient depletion as they grow (e.g., Doney, 2006). Additionally, this process (thermal stratification) can lead to less upwelling and weaker inshore transport at depth which may, ultimately, reduce the available nutrients (Platt et al., 2005).

In this study, the main physical mechanisms controlling phytoplankton biomass (and hence squid catch) were wind and wind-driven upwelling. This is coherent with the findings of Jury (2019), who showed that October–March winds favoured upwelling over the Eastern Agulhas Bank (Jury, 2019). In their work, salinity (not examined here) was found to be another productivity factor over the Eastern Agulhas Bank (Jury, 2019). Other potential controls such as turbidity events which have also been identified as a factor reducing squid reproduction (e.g., Roberts and Sauer, 1994; Roberts, 1998), are not investigated in

this study. Also, factors such as surface currents are less explored and should be further addressed in future work. This is especially relevant since changes in the AC were found to influence aggregate fish catch along the south coast of South Africa (Jury, 2011) and south-westward currents to favour squid catch along the Eastern Agulhas Bank (Jury, 2019). One question worth exploring is how the different AC modes would impact the seasonal upwelling over the bank, given that squid paralarval distribution might be influenced by the currents' behaviour on the Agulhas Bank (Lipiński et al., 2016 and references therein). A more holistic approach may integrate climate variability modes which often trigger perturbations in atmospheric forcing and affect trophic levels of marine ecosystems (Chavez et al., 2003; Behrenfeld et al., 2006). For example, the El Niño-Southern Oscillation (ENSO) and the Southern Annular Mode (SAM) have been linked to the Agulhas Current transport variance (Elipot and Beal, 2018) and coastal upwelling on the Agulhas Bank (Malan et al., 2019). It has also been shown that El-Niño can influence primary production along the South African coast (Racault et al., 2017). Exploring the connection of climate indices and large-scale atmospheric forcing to coastal wind changes, as well as their impact on marine ecosystems, would require the use of a coupled ocean-atmosphere model (Malan et al., 2019), further coupled with models of marine biogeochemistry and ecosystems.

5. Conclusions & perspectives

This study provides the first long-term analysis of chokka squid catch variations in relation to biophysical indicators in South African waters based on twenty years (1998–2017) of satellite observations. The annual squid catch is significantly positively correlated to remotely-sensed annual *Chl-a*, and both variables oscillate in phase from year to year over the Agulhas Bank and the South African west coast. This region experiences two seasonal blooms in autumn (March–May) and spring (September–November), with maximum *Chl-a* reached in April and October, respectively. These phytoplankton blooms show drastic *Chl-a* declines during the squid catch declines of 2001 and 2013, while elevated *Chl-a* levels are observed during the high catch years of 2004 and 2009.

Spatial correlations show that phytoplankton availability in the study region is closely linked to physical controls (winds, SST, surface currents) during Oct–Apr. *Chl-a* appears highly influenced by local wind forcing, with the occurrence of wind-driven upwellings (a combination of Ekman transport due to the north-westward/westward winds and Ekman suction via negative wind stress curl) over the South African west coast and the central Agulhas Bank (i.e., Benguela and Cold Ridge upwellings areas). The *Chl-a* – SST and – current speed relationships show the currents being more significant for shelf edge processes and likely for advection along the Cold Ridge pathway on shorter timescales (December–February), contributing alongside the winds to more nutrients and phytoplankton growth.

The years of very low squid catch are linked to low *Chl-a* regimes driven by weak winds and relaxed WSC(–) over the Benguela upwelling zone (southwest coast) in 2001 and both Benguela upwelling and Cold Ridge (central Agulhas Bank) zones in 2013. Additionally, the phytoplankton phenology (timing of growth) indicates low phytoplankton (food) availability with absent or shorter and delayed blooms over the Benguela upwelling area in 2001 and both Benguela and Cold Ridge upwelling areas in 2013. The high catches of 2004 and 2009, associated with elevated *Chl-a*, were induced by strong winds over the Benguela and Cold Ridge areas in 2004, and by intensified WSC(–) over the Benguela upwelling area in 2009. The high catches of 2004 and 2009 coincided with early and/or prolonged seasonal blooms which may be indicative of enhanced larval survival over the Benguela and Cold Ridge upwelling zones.

In view of the difficulty of maintaining a dense and cost-effective *in situ* network in the region, satellite-derived data can be a useful tool to obtain environmental and ecological indicators, influencing fishery

resources and addressing specific management objectives. The weak wind-induced upwellings, low *Chl-a* regimes and anomalous alterations in bloom phenology, such as in 2001 and 2013, are likely to occur in the future given that squid is a short-lived species which renders it vulnerable to environmental and climate change (Glazer et al., 2012; Zantsi et al., 2013). These potential scenarios of low productivity and squid catch can be anticipated using near-real-time satellite data which can be directly linked to the catch through phytoplankton biomass. Although the bloom metrics of specific years may change more often than normal due to the heterogenous dynamics of the region, the climatological phenology indices, for example (Table 1), can serve as a benchmark for anomalous blooms and thus catches. We suggest that the management authority (DFFE) and the industry (through the South African Squid Management Industrial Association) may benefit from including an early warning system in the current management of the squid fishery that integrates *Chl-a*, phenology metrics and wind data which have proved effective in detecting low productivity conditions. Such predictability tools could help the management of the resource and promote adaptive measures against economic repercussions.

CRedit authorship contribution statement

Fatma Jebri: Conceptualization, Investigation, Formal analysis, Visualization, Software, Writing – original draft, Writing – review & editing. **Dionysios E. Raitsos:** Conceptualization, Methodology, Validation, Writing – review & editing. **John A. Gittings:** Formal analysis, Software, Data curation, Writing – review & editing. **Zoe L. Jacobs:** Conceptualization, Writing – review & editing. **Meric Srokosz:** Conceptualization, Supervision, Validation, Writing – review & editing. **Jessica Gornall:** Resources, Writing – review & editing. **Warwick H.H. Sauer:** Writing – review & editing. **Michael J. Roberts:** Funding acquisition, Project administration, Writing – review & editing. **Eka-terina Popova:** Funding acquisition, Project administration, Supervision, Writing – review & editing.

Declaration of competing interest

The authors declare that they have no known competing financial interests or personal relationships that could have appeared to influence the work reported in this paper.

Acknowledgments

The study was supported by the Global Challenges Research Fund (GCRF) under NERC grant NE/P021050/1 in the framework of the SOLSTICE-WIO project (<https://www.solstice-wio.org/>). The satellite SST and the altimetry-derived absolute geostrophic currents were distributed by the Copernicus Marine Environment Monitoring Service (CMEMS) (<http://www.marine.copernicus.eu>). We thank the ESA Ocean Colour CCI project for processing and providing the *Chl-a* dataset online at <http://www.esa-oceancolour-cci.org/>. We acknowledge the European Centre for Medium-Range Weather Forecasts (ECMWF) for producing and the Climate Data Store (CDS) for distributing the ERA-5 wind dataset. We thank the South African Department of Forestry, Fisheries and the Environment (DFFE) for providing the squid catch data. Michael J. Roberts and Jessica Gornall are partly funded by the joint National Research Foundation (NRF) – British Council, Newton Fund Grant SARChI 150326116102/NRF 98399. John A. Gittings was supported by a grant from the Living Planet Fellowship of the European Space Agency (POSEIDON/14-03-2021).

Appendix A. Supplementary data

Supplementary data to this article can be found online at <https://doi.org/10.1016/j.dsr2.2022.105028>.

References

- Augustyn, C.J., 1990. Biological studies on the Chokka squid *Loligo vulgaris reynaudii* (Cephalopoda; Myopsida) on spawning grounds off the south-east coast of South Africa. *S. Afr. J. Mar. Sci.* 9 (1), 11–26. <https://doi.org/10.2989/025776190784378736>.
- Augustyn, C.J., 1991. The biomass and ecology of Chokka squid *Loligo vulgaris reynaudii* off the West Coast of South Africa. *S. Afr. J. Zool.* 26 (4), 164–181. <https://doi.org/10.1080/02541858.1991.11448245>.
- Augustyn, C.J., Llipinski, M.R., Sauer, W.H.H., 1992. Can the Loligo squid fishery be managed effectively? A synthesis of research on *Loligo vulgaris reynaudii*. *S. Afr. J. Mar. Sci.* 12 (1), 903–918. <https://doi.org/10.2989/02577619209504751>.
- Augustyn, C.J., Lipinski, M.R., Sauer, W.H.H., Roberts, M.J., Mitchell-Innes, B.A., 1994. Chokka squid on the Agulhas Bank: life history and ecology. *South Afr. J. Sci.* 90 (3), 143–154. <http://oceanrep.geomar.de/38169/1/2854.pdf>.
- Augustyn, J., Cockcroft, A., Kerwath, S., Lamberth, S., Githaiga-Mwici, J., Pitcher, G., Roberts, M., Van der Lingen, C., Auerswald, L., 2017. South Africa. In: *Climate Change Impacts on Fisheries and Aquaculture* (Eds B.F. Phillips and M. Pérez-Ramírez). <https://doi.org/10.1002/9781119154051.ch15>.
- Bakun, A., Roy, C., Luch-Cota, S., 1998. Coastal upwelling and other processes regulating ecosystem productivity and fish production in the western Indian Ocean. In: *Large Marine Ecosystems of the Indian Ocean: Assessment, Sustainability and Management*. (Eds. Sherman K., Okemwa E.N., Ntiba M.J., Blackwell, pp. 103–141. https://horizon.documentation.ird.fr/exl-doc/pleins_textes/pleins_textes_7/b_fdi_57-58/010025378.pdf.
- Bakun, A., Black, B.A., Bograd, S.J., Garcia-Reyes, M., Miller, A.J., Rykaczewski, R.R., Sydeman, W.J., 2015. Anticipated effects of climate change on coastal upwelling ecosystems. *Curr. Clim. Change Rep.* 1 (2), 85–93. <https://doi.org/10.1007/s40641-015-0008-4>.
- Beal, L.M., Bryden, H.L., 1999. The velocity and vorticity structure of the Agulhas Current at 32°S. *J. Geophys. Res.* 104:C3 5151–5176. [10.1029/1998JC900056](https://doi.org/10.1029/1998JC900056).
- Beal, L.M., De Ruijter, W.P.M., Biastoch, A., Zahn, R., 2011. On the role of the Agulhas system in ocean circulation and climate. *Nature* 472 (7344), 429–436. <https://doi.org/10.1038/nature09983>.
- Behrenfeld, M.J., O'Malley, R.T., Siegel, D.A., McClain, C.R., Sarmiento, J.L., Feldman, G.C., Milligan, A.J., Falkowski, P.G., Letelier, R.M., Boss, E.S., 2006. Climate-driven trends in contemporary ocean productivity. *Nature* 444, 752–755. <https://doi.org/10.1038/nature05317>.
- Boyd, A., Shillington, F., 1994. Physical forcing and circulation patterns on the Agulhas Bank. *South Afr. J. Sci.* 90, 114–122. <https://journals.co.za/doi/pdf/10.10520/AJA00382353.4624>.
- Briceño, H.O., Boyer, J.N., 2010. Climatic controls on phytoplankton biomass in a subtropical estuary, Florida Bay, USA. *Estuar. Coast* 33, 541–553. <https://doi.org/10.1007/s12237-009-9189-1>.
- Chassot, E., Bonhommeau, S., Reygondeau, G., Nieto, K., Polovina, J.J., Huret, M., Dulvy, N.K., Demarcq, H., 2011. Satellite remote sensing for an ecosystem approach to fisheries management. *ICES (Int. Counc. Explor. Sea) J. Mar. Sci.* 68 (4), 651–666. <https://doi.org/10.1093/icesjms/fsq195>.
- Chavez, F.P., Ryan, J., Lluch-Cota, S.E., Niquen, M.C., 2003. From anchovies to sardines and back: multidecadal change in the Pacific Ocean. *Science* 299, 217–221. [10.1126/science.1075880](https://doi.org/10.1126/science.1075880).
- Cochrane, K.L., Oliver, B., Sauer, W., 2014. An assessment of the current status of the Chokka squid fishery in South Africa and an evaluation of alternative allocation strategies. *Mar. Pol.* 43, 149–163. <https://doi.org/10.1016/j.marpol.2013.05.006>.
- Cole, H.S., 2014. *The Natural Variability and Climate Change Response in Phytoplankton Phenology*. Doctoral Dissertation. University of Southampton.
- DAFF, 2009. 2009/10 DAFF Strategic Plan. Department of Agriculture Forestry and Fisheries, Pretoria.
- DAFF, 2013. Draft revised squid policy on the allocation and management of fishing rights. https://www.nda.agric.za/doiDev/sideMenu/fisheries/21_HotIssues/Apri12010/AllocationOfRights/Draft%20revised%20SQUID%20POLICY%20May%202013.pdf, 2013.
- DEAT, 2005. Policy for the Allocation and Management of Commercial Fishing Rights in the Squid Fishery. Department of Environmental Affairs and Tourism, Pretoria. https://www.nda.agric.za/doiDev/sideMenu/fisheries/13_PerformanceReviews/policies/Cluster%20B%20policies/05_-_Squid_Policy_English.pdf.
- Dencausse, G., Arhan, M., Speich, S., 2010. Spatio-temporal characteristics of the Agulhas current retroflection. *Deep-Sea Res. Part I Oceanogr. Res. Pap.* 57 (11), 1392–1405. <https://doi.org/10.1016/j.dsr.2010.07.004>.
- D'Errico, J., 2012. Interpolate NaN elements in a 2D array using non-NaN elements. MATLAB. Cent. File Exch. https://www.mathworks.com/matlabcentral/fileexchange/4551-inpaint_nans.
- Desbiolles, F., Blanke, B., Bentamy, A., Grima, N., 2014. Origin of fine-scale wind stress curl structures in the Benguela and Canary upwelling systems. *J. Geophys. Res. Oceans* 119, 7931–7948. [10.1002/2014JC010015](https://doi.org/10.1002/2014JC010015).
- Downey, N.J., Roberts, M.J., Baird, D., 2010. An investigation of the spawning behaviour of the Chokka squid *Loligo reynaudii* and the potential effects of temperature using acoustic telemetry. *ICES (Int. Counc. Explor. Sea) J. Mar. Sci.* 67, 231–243. <https://academic.oup.com/icesjms/article/67/2/231/693114>.
- Doney, S., 2006. Plankton in a warmer world. *Nature* 695–696. <https://doi.org/10.1038/444695a>.
- Elipot, S., Beal, L.M., 2015. Characteristics, energetics, and origins of Agulhas current meanders and their limited influence on Ring Shedding. *J. Phys. Oceanogr.* 45 (9), 2294–2314. <https://journals.ametsoc.org/view/journals/phoc/45/9/jpo-d-14-0254.1.xml>.
- Elipot, S., Beal, L.M., 2018. Observed Agulhas current sensitivity to interannual and long-term trend atmospheric forcings. *J. Clim.* 31 (8), 3077–3098. <https://journals.ametsoc.org/view/journals/clim/31/8/jcli-d-17-0597.1.xml>.
- FAO, 2016. AQUASTAT Country Profile – South Africa. Food and Agriculture Organization of the United Nations (FAO), Rome, Italy. <http://www.fao.org/3/i9821en/19821EN.pdf>.
- Froese, R., Zeller, D., Kleisner, K., Pauly, D., 2012. What catch data can tell us about the status of global fisheries. *Mar. Biol.* 159, 1283–1292. [10.1007/s00227-012-1909-6](https://doi.org/10.1007/s00227-012-1909-6).
- Gill, A.E., 1982. *Atmosphere-Ocean Dynamics*. Academic, San Diego, Calif. <https://www.elsevier.com/books/atmosphere-ocean-dynamics/gill/978-0-12-283522-3>.
- Gittings, J.A., Raitso, D.E., Krokos, G., Hoteit, I., 2018. Impacts of warming on phytoplankton abundance and phenology in a typical tropical marine ecosystem. *Sci. Rep.* 8 (2240) <https://doi.org/10.1038/s41598-018-20560-5>.
- Gittings, J.A., Raitso, D.E., Kheirredine, M., Racault, M.F., Claustre, H., Hoteit, I., 2019. Evaluating tropical phytoplankton phenology metrics using contemporary tools. *Sci. Rep.* 9 (674) <https://doi.org/10.1038/s41598-018-37370-4>.
- Gittings, J.A., Raitso, D.E., Brewin, R.J.W., Hoteit, I., 2021. Links between phenology of large phytoplankton and fisheries in the northern and central red Sea. *Rem. Sens.* 13 (231) <https://doi.org/10.3390/rs13020231>.
- Glazer, J.P., Durholtz, D., Van Der Westhuizen, J., 2012. *Background Information to the South African Squid Resource Loligo Reynaudii*. Department of Agriculture, Forestry and Fisheries, Cape Town.
- Hecky, R.E., Kilham, P., 1988. Nutrient limitation of phytoplankton in freshwater and marine environments: a review of recent evidence on the effects of enrichment. *Limnol. Oceanogr.* 33 (4), 796–822. <https://doi.org/10.4319/lo.1988.33.4part2.0796>.
- Hersbach, H., Bell, B., Berrisford, P., Biavati, G., Horányi, A., Muñoz Sabater, J., Nicolas, J., Peubey, C., Radu, R., Rozum, I., Schepers, D., Simmons, A., Soci, C., Dee, D., Thépaut, J.-N., 2019. ERA5 monthly averaged data on single levels from 1979 to present. Copernicus Climate Change Service (C3S) Climate Data Store (CDS). <https://doi.org/10.24381/cds.fl705d07>. (Accessed 3 February 2021).
- Hutchings, L., Beckley, L.E., Griffiths, M.H., Roberts, M.J., Sundby, S., Van der Lingen, C., 2002. Spawning on the edge: spawning grounds and nursery areas around the southern African coastline. *Mar. Freshw. Res.* 53, 307–318. <https://doi.org/10.1071/MF01147>.
- Hutchings, L., 1994. The Agulhas Bank: a synthesis of available information and a brief comparison with other east-coast shelf regions. *S. Afr. J. Sci.* 90, 179–185. <https://hdl.handle.net/10520/AJA00382353.4628>.
- IOCCG, 2000. *Remote sensing of ocean colour in coastal and other optically complex waters*. In: *Reports of the International Ocean Colour Coordinating Group Number 3*. Sathyendranath, Dartmouth, Canada), 140.
- Jackson, J.M., Rainville, L., Roberts, M.J., McQuaid, C.D., Lutjeharms, J.R., 2012. Mesoscale bio-physical interactions between the Agulhas current and the Agulhas Bank, South Africa. *Contin. Shelf Res.* 49, 10–24. <https://doi.org/10.1016/j.csr.2012.09.005>.
- Jackson, T., Sathyendranath, S., Mélin, F., 2017. An improved optical classification scheme for the Ocean Colour Essential Climate Variable and its applications. *Remote Sens. Environ.* 203, 152–161. <https://doi.org/10.1016/j.rse.2017.03.036>.
- Jacobs, Z.L., Roberts, M.J., Jebri, F., Srokosz, M., Kelly, S., Asdar, S., Sauer, W.H.H., Popova, E. This issue. Drivers of productivity on the Agulhas Bank and the importance for marine ecosystems.
- Jebri, F., Jacobs, Z.L., Raitso, D.E., Srokosz, M., Painter, S.C., Kelly, S., Roberts, M.J., Scott, L., Taylor, S.F.W., Palmer, M., Kizenga, H., Shaghude, Y., Whiggott, J., Popova, E., 2020. Interannual monsoon wind variability as a key driver of East African small pelagic fisheries. *Sci. Rep.* 10 <https://doi.org/10.1038/s41598-020-70275-9>.
- Joyner, J.M., 2015. *The Influence of Environmental Variability on the Catch of Chokka, loligo reynaudii, off the Coast of South Africa*. Master's Thesis. Rhodes University, South Africa. <http://vital.seals.ac.za:8080/vital/access/manager/PdViewer/vital:24013/SOURCE1?viewPdfInternal=1>.
- Junker, T., Schmidt, M., Mohrholz, V., 2015. The relation of wind stress curl and meridional transport in the Benguela upwelling system. *J. Mar. Syst.* 143, 1–6. <https://doi.org/10.1016/j.jmarsys.2014.10.006>.
- Jury, M.R., 2011. Environmental influences on South African fish catch: south Coast transition. *Int. J. Oceanogr.* 920414, 1687–9406. <https://doi.org/10.1155/2011/920414>.
- Jury, M.R., 2019. Environmental controls on marine productivity near Cape St. Francis, South Africa. *Ocean Sci.* 15, 1579–1592. <https://doi.org/10.5194/os-15-1579-2019>.
- Kassi, J.B., Racault, M.F., Mobio, B.A., Platt, T., Sathyendranath, S., Raitso, D.E., Affian, K., 2018. Remotely sensing the biophysical drivers of *Sardinella aurita* variability in ivorian waters. *Rem. Sens.* 10 (785) <https://doi.org/10.3390/rs10050785>.
- Kizenga, H.J., Jebri, F., Shaghude, Y., Raitso, D.E., Srokosz, M., Jacobs, Z.L., Nencioli, F., Shalli, M., Kyewalyanga, M.S., Popova, E., 2021. Variability of mackerel fish catch and remotely-sensed biophysical controls in the eastern Pemba channel. *Ocean Coast Manag.* 207, 105593. <https://doi.org/10.1016/j.ocecoaman.2021.105593>.
- Krug, M., Tournadre, J., Dufois, F., 2014. Interactions between the Agulhas current and the eastern margin of the Agulhas Bank. *Contin. Shelf Res.* 81, 67–79. <https://doi.org/10.1016/j.csr.2014.02.020>.
- Krug, M., Swart, S., Gula, J., 2017. Submesoscale cyclones in the Agulhas current. *Geophys. Res. Lett.* 44, 346–354. <https://doi.org/10.1002/2016GL071006>.
- Lam, V.W.Y., Tavakolie, A., Pauly, D., Zeller, D., 2015. The Sea Around Us databases and their spatial dimensions. In: *Catch Reconstructions: Concepts, Methods and Data Sources* (Eds. Pauly, D. & Zeller, D. University of British Columbia).

- Large, W.G., Pond, S., 1981. open ocean momentum flux measurements in moderate to strong winds. *J. Phys. Oceanogr.* 11 (3), 324–336. https://journals.ametsoc.org/view/journals/phoc/11/3/1520-0485_1981_011_0324_oomfmi_2_0_co_2.xml.
- Leber, G.M., Beal, L.M., Elipot, S., 2017. Wind and current forcing combine to drive strong upwelling in the Agulhas current. *J. Phys. Oceanogr.* 47 (1), 123–134. <https://journals.ametsoc.org/view/journals/phoc/47/1/jpo-d-16-0079.1.xml>.
- Lipiński, M.R., 1994. Differences among basic biological parameters in a population of Chokka squid *Loligo vulgaris reynaudii* (Cephalopoda: loliginidae) sampled by three methods. *S. Afr. J. Mar. Sci.* 14, 281–286. <https://doi.org/10.2989/025776194784287021>.
- Lipiński, M.R., Van der Vyver, J.S.F., Shaw, P., Sauer, W.H.H., 2016. Life cycle of Chokka-squid *Loligo reynaudii* in South African waters. *Afr. J. Mar. Sci.* 38 (4), 589–593. <https://doi.org/10.2989/1814232X.2016.1230074>.
- Lipiński, M.R., Mwanangombe, C.H., Durholtz, D., Yemane, D., Githaiga-Mwici, J., Sauer, W.H.H., 2020. Age estimates of Chokka squid *Loligo reynaudii* off South Africa and their use to test the effectiveness of a closed season for conserving this resource. *Afr. J. Mar. Sci.* 42 (4), 461–471. <https://doi.org/10.2989/1814232X.2020.1842804>.
- Liuzzo, L., Bono, E., Sammartano, V., Freni, G., 2017. Long-term temperature changes in sicily, southern Italy. *Atmos. Res.* 198, 44–55. <https://doi.org/10.1016/j.atmosres.2017.08.007>.
- Lutjeharms, J.R.E., Catzel, R., Valentine, H.R., 1989. Eddies and other boundary phenomena of the Agulhas Current. *Continent. Shelf Res.* 9, 597–616. [https://doi.org/10.1016/0278-4343\(89\)90032-0](https://doi.org/10.1016/0278-4343(89)90032-0).
- Lutjeharms, J.R.E., Penven, P., Roy, C., 2003. Modelling the shear edge eddies of the southern Agulhas Current. *Continent. Shelf Res.* 23 (11–13), 1099–1115. [https://doi.org/10.1016/S0278-4343\(03\)00106-7](https://doi.org/10.1016/S0278-4343(03)00106-7).
- Lutjeharms, J.R.E., 2006. The Agulhas current, Springer Berlin Heidelberg. <https://doi.org/10.1007/3-540-37212-1>.
- Lutjeharms, J.R.E., 2007. Three decades of research on the greater Agulhas Current. *Ocean Sci.* 3, 129–147. <https://doi.org/10.5194/os-3-129-2007>.
- Malan, N., Backeberg, B., Biastoch, A., Durgadoo, J.V., Samuelsen, A., Reason, C., Hermes, J., 2018. Agulhas current meanders facilitate shelf-slope exchange on the eastern Agulhas Bank. *J. Geophys. Res.* 123 (7), 4762–4778. <https://doi.org/10.1029/2017JC013602>.
- Malan, N.C., Durgadoo, J.V., Biastoch, A., Reason, C.J., Hermes, J.C., 2019. Multidecadal wind variability drives temperature shifts on the Agulhas Bank. *J. Geophys. Res.* 124, 3021–3035. <https://doi.org/10.1029/2018JC014614>.
- Manly, B.F.J., MacKenzie, D., 2000. A cumulative sum type of method for environmental monitoring. *Environmetrics* 11, 151–166. [10.1002/\(SICI\)1099-095X\(200003/04\)11:2<151::AID-ENV394>3.0.CO;2-B](https://doi.org/10.1002/(SICI)1099-095X(200003/04)11:2<151::AID-ENV394>3.0.CO;2-B).
- Martinez, E., Antoine, D., D'Ortenzio, F., De Boyer Montegut, C., 2011. Phytoplankton spring and fall blooms in the north atlantic in the 1980s and 2000s. *Journal of geophysical research.* 116, C11029. <https://doi.org/10.1029/2010JC006836>.
- Matano, R., May 2020. The Agulhas Bank circulation. EGU general assembly 2020. Online 4–8. <https://doi.org/10.5194/egusphere-egu2020-3153>.
- Matano, R.P., Combes, V., Strub, P.T., James, C., 2020. 2020 Ocean Surface topography science team meeting, science II: large scale ocean circulation variability and change. https://ostst.avisio.altimetry.fr/fileadmin/user_upload/tx_ausyclese_minar/files/MATANO_AVISO.pdf.
- Mthembu, S.P., 2019. The Socio-Economic Impact of the Squid Stock Volatility in the Eastern Cape Province of South Africa. Master's Thesis. University of Cape Town, School of Economics, South Africa, p. 52. https://open.uct.ac.za/bitstream/handle/11427/31078/thesis_com_2019_mthembu_senzo_peter.pdf?isAllowed=y&sequence=1.
- Mazwane, S.L., Poulton, A.J., Hickman, A., Jebri, F., Jacobs, Z., Roberts, M.J., Noyon, M., 2018. Seasonal and long-term stability of net primary production on the agulhas bank, 1998–2018.
- McQuatters-Gollop, A., Mee, L.D., Raitos, D.E., Shapiro, G.I., 2008. Non-linearities, regime shifts and recovery: the recent influence of climate on Black Sea chlorophyll. *J. Mar. Syst.* 74, 649–658. <https://doi.org/10.1016/j.jmarsys.2008.06.002>.
- Mwici, J., Durholtz, D., Glazer, J., Butterworth, D., 2018. Considerations on Management of the Chokka Squid Jig Fishery with Reference to the Pending FRAP 2020 Allocation of Fishing Rights and Implementation of Small Scale Fisheries. FISHERIES/2018/AUGUST/SWG-SQ/17. Department of Agriculture, Forestry and Fisheries (DAFF). South Africa, Cape Town. https://open.uct.ac.za/bitstream/handle/11427/30228/FISHERIES_2018_AUGUST_Squid_SWG-SQ17_Research%20Inputs%20into%20the%20Squid%202020%20FRAP_Final.pdf?sequence=1&isAllowed=y.
- Olyott, L.J.H., Sauer, W.H.H., Booth, A.J., 2006. Spatio-temporal patterns in maturation of the Chokka squid (*Loligo vulgaris reynaudii*) off the coast of South Africa. *ICES (Int. Counc. Explor. Sea) J. Mar. Sci.* 63 (9), 1649–1664. <https://doi.org/10.1016/j.icesjms.2006.06.011>.
- Olyott, L.J.H., Sauer, W.H.H., Booth, A.J., 2007. Spatial patterns in the biology of the Chokka squid, *Loligo reynaudii* on the Agulhas Bank. *South Africa. Rev. Fish. Biol. Fisheries* 17, 159–172. <https://doi.org/10.1007/s11160-006-9027-5>.
- Oosthuizen, A., Roberts, M.J., Sauer, W.H.H., 2002. Temperature effects on the embryonic development and hatching success of the squid *Loligo vulgaris reynaudii*. *Bull. Mar. Sci.* 71, 619–632.
- Paldor, N., Lutjeharms, J.R.E., 2009. Why is the stability of the Agulhas Current geographically bi-modal? *Geophys. Res. Lett.* 36 (14) <https://doi.org/10.1029/2009GL038445>.
- Pauly, D., Zeller, D., 2016. Catch reconstructions reveal that global marine fisheries catches are higher than reported and declining. *Nat. Commun.* 7, 10244.
- Pauly, D., Zeller, D., 2018. Agreeing with FAO: comments on SOFIA 2018. *Mar. Pol.* 100, 332–333. <https://doi.org/10.1016/j.marpol.2018.12.009>.
- Penven, P., Lutjeharms, J., Marchesiello, P., Roy, C., Weeks, S., 2001. Generation of cyclonic eddies by the Agulhas current in the lee of the Agulhas Bank. *Geophys. Res. Lett.* 28, 1055–1058. <https://doi.org/10.1029/2000GL01760>.
- Pickett, M.H., Paduan, J.D., 2003. Ekman transport and pumping in the California Current based on the U.S. Navy's high-resolution atmospheric model (COAMPS). *J. Geophys. Res.* 108 (C10) <https://doi.org/10.1029/2003JC001902>.
- Platt, T., Sathyendranath, S., 2008. Ecological indicators for the pelagic zone of the ocean from remote sensing. *Remote Sens. Environ.* 112, 3426–3436. <https://doi.org/10.1016/j.rse.2007.10.016>.
- Platt, T., Fuentes-Yaco, C., Frank, K., 2003. Spring algal bloom and larval fish survival. *Nature* 423, 398–399. <https://doi.org/10.1038/423398b>.
- Platt, T., Bouman, H., Devred, E., Fuentes-Yaco, C., Sathyendranath, S., 2005. Physical forcing and phytoplankton distributions. *Sci. Mar.* 69, 55–73. <https://scientiamarina.revistas.csic.es/index.php/scientiamarina/article/view/294/294>.
- Platt, T., White, G.N., Zhai, L., Sathyendranath, S., Roy, S., 2009. The phenology of phytoplankton blooms: ecosystem indicators from remote sensing. *Ecol. Modell.* 220, 3057–3069. <https://doi.org/10.1016/j.ecolmodel.2008.11.022>.
- Racault, M.F., Le Quéré, C., Buitenhuis, E., Sathyendranath, S., Platt, T., 2012. Phytoplankton phenology in the global ocean. *Ecolog. Indic.* 14, 152–163. <https://doi.org/10.1016/j.ecolind.2011.07.010>.
- Racault, M.F., Raitos, D.E., Berumen, M.L., Brewin, R.J.W., Platt, T., Sathyendranath, S., Hoteit, I., 2015. Phytoplankton phenology indices in coral reef ecosystems: application to ocean-color observations in the Red Sea. *Remote Sens. Environ. Times* 160, 222–234. <https://doi.org/10.1016/j.rse.2015.01.019>.
- Racault, M.F., Sathyendranath, S., Brewin, R.J.W., Raitos, D.E., Jackson, T., Platt, T., 2017. Impact of El Niño variability on oceanic phytoplankton. *Front. Mar. Sci.* 4 (133) <https://doi.org/10.3389/fmars.2017.00133>.
- Raitos, D.E., Pradhan, Y., Brewin, R.J., Stenichikov, G., Hoteit, I., 2013. Remote sensing the phytoplankton seasonal succession of the Red Sea. *PLoS One* 8, e64909. <https://doi.org/10.1371/journal.pone.0064909>.
- Raitos, D.E., Pradhan, Y., Lavender, S., Hoteit, I., McQuatters-Gollop, A., Reid, P.C., Richardson, A., 2014. From silk to satellite: half a century of ocean colour anomalies in the Northeast Atlantic. *Global Change Biol.* 20, 2117–2123. <https://doi.org/10.1111/gcb.12457>.
- Raitos, D.E., Yi, X., Platt, T., Racault, M.F., Brewin, R.J.W., Pradhan, Y., Papadopoulos, V.P., Sathyendranath, S., Hoteit, I., 2015. Monsoon oscillations regulate fertility of the Red Sea. *Geophys. Res. Lett.* 42, 855–862. <https://doi.org/10.1002/2014GL028822>.
- Raitos, D.E., Brewin, R.J.W., Zhan, P., Dreano, D., Pradhan, Y., Nanninga, G.B., Hoteit, I., 2017. Sensing coral reef connectivity from space. *Sci. Rep.* 7 (9338) <https://doi.org/10.1038/s41598-017-08729-w>.
- Regier, P., Briceño, H., Boyer, J.N., 2019. Analyzing and comparing complex environmental time series using a cumulative sums approach. *MethodsX* 6, 779–787. <https://doi.org/10.1016/j.mex.2019.03.014>.
- Renault, L., McWilliams, J.C., Masson, S., 2017. Satellite observations of imprint of oceanic current on wind stress by air-sea coupling. *Sci. Rep.* 7, 17747. <https://doi.org/10.1038/s41598-017-17939-1>.
- Risien, C.M., Chelton, D.B., 2008. A global climatology of surface wind and wind stress fields from eight years of QuikSCAT scatterometer data. *J. Phys. Oceanogr.* 38, 2379–2413. [10.1175/2008JPO3881.1](https://doi.org/10.1175/2008JPO3881.1).
- Roberts, M.J., Sauer, W.H.H., 1994. Environment: the key to understanding the South African Chokka squid (*Loligo vulgaris reynaudii*) life cycle and fishery. *Antarct. Sci.* 6, 249–258.
- Roberts, M.J., Van den Berg, M., 2002. Recruitment variability of Chokka squid (*Loligo vulgaris reynaudii*)—role of currents on the Agulhas Bank (South Africa) in paralarvae distribution and food abundance. *Bull. Mar. Sci.* 71 (2), 691–710. <https://doi.org/10.1017/S0954102094000386>.
- Roberts, M.J., 1998. The influence of the environment on Chokka squid *Loligo vulgaris reynaudii* spawning aggregations: steps towards a quantified model. *S. Afr. J. Mar. Sci.* 20, 267–284. <https://doi.org/10.2989/025776198784126223>.
- Roberts, M.J., 2005. Chokka squid (*Loligo vulgaris reynaudii*) abundance linked to changes in South Africa's Agulhas Bank ecosystem during spawning and the early life cycle. *ICES (Int. Counc. Explor. Sea) J. Mar. Sci.* 62 (1), 33–55. <https://doi.org/10.1016/j.icesjms.2004.10.002>.
- Roel, B., Butterworth, D.S., 2000. Assessment of the South African Chokka squid *Loligo vulgaris reynaudii*. Is disturbance of aggregations by the recent jig fishery having a negative impact on recruitment? *Fish. Res.* 48, 213–228.
- Russo, C.S., Lamont, T., Krug, M., 2021. Spatial and temporal variability of the Agulhas Retroflection: observations from a new objective detection method. *Remote Sens. Environ.* 253, 112239. <https://doi.org/10.1016/j.rse.2020.112239>.
- Sathyendranath, S., Jackson, T., Brockmann, C., Brotas, V., Calton, B., Chuprin, A., Clements, O., Cipollini, P., Danne, O., Dingle, J., Donlon, C., Grant, M., Groom, S., Krasemann, H., Lavender, S., Mazeran, C., Mélin, F., Moore, T.S., Müller, D., Regner, P., Steinmetz, F., Steele, C., Swinton, J., Valente, A., Zühlke, M., Feldman, G., Franz, B., Frouin, R., Werdell, J., Platt, T., 2020. ESA ocean colour climate change initiative (Ocean Colour_cci): global ocean colour data products gridded on a geographic projection (all products), version 4.2. Centre for environmental data analysis. <https://catalogue.ceda.ac.uk/uuid/aeae1a19608347f7b802691db6984343>.
- Sauer, W.H.H., Lipinski, M.R., 1991. Food of squid *Loligo vulgaris reynaudii* (Cephalopoda: Loliginidae) on their spawning grounds off the Eastern Cape, South Africa. *S. Afr. J. Mar. Sci.* 10, 193–201. <https://doi.org/10.2989/02577619109504631>.
- Sauer, W.H.H., Smale, M.J., Lipinski, M.R., 1992. The location of spawning grounds, spawning and schooling behaviour of the squid *Loligo vulgaris reynaudii*

- (Cephalopoda: myopsida) off the Eastern Cape Coast, South Africa. *Mar. Biol.* 114, 97–107. <https://doi.org/10.1007/BF00350859>.
- Sauer, W.H.H., Downey, N.J., Lipiński, M., Roberts, M.J., Smale, M.J., Shaw, P., Glazer, J., Melo, Y., 2013. *Loligo reynaudii*, Chokka squid. In: *Advances in Squid Biology, Ecology and Fisheries. Part I – Myopsid Squids*. (Rosa R, O'Dor R, Pierce G eds., Hauppauge, New York. Nova Science Publishers Inc, pp. 33–71.
- Schumann, E., 1999. Wind-driven mixed layer and coastal upwelling processes off the south coast of South Africa. *J. Mar. Res.* 57, 671–691. [10.1357/002224099321549639](https://doi.org/10.1357/002224099321549639).
- Shannon, L.V., Hutchings, L., Bailey, G.W., Shelton, P.A., 1984. Spatial and temporal distribution of chlorophyll in southern African waters as deduced from ship and satellite measurements and their implications for pelagic fisheries. *S. Afr. J. Mar. Sci.* 2 (1), 109–130. <https://doi.org/10.2989/02577618409504363>.
- Siegel, D.A., Doney, S.C., Yoder, J.A., 2002. The North Atlantic spring phytoplankton bloom and Sverdrup's critical depth hypothesis. *Science* 296 (5568), 730–733. <https://doi.org/10.1126/science.1069174>.
- Stats, S.A., 2020. http://www.statssa.gov.za/?page_id=737&id=1#national_qes.
- Strub, P.T., James, C., Matano, R.P., Combes, V., 2020. Ocean Surface topography science team meeting, science II: large scale ocean circulation variability and change, 2020. https://ostst.avisio.altimetry.fr/fileadmin/user_upload/tx_ausyclsseminar/files/Strub2b-Benguela-Agulhas-Altimeter-LS-Circ.pdf, 2020.
- Taylor, A., Allen, J., Clark, P., 2002. Extraction of a weak climatic signal by an ecosystem. *Nature* 416, 629–632. <https://doi.org/10.1038/416629a>.
- Tilstone, G.H., Xie, Y., Robinson, C., Serret, P., Raitos, D.E., Powell, T., Aranguren-Gassis, M., Garcia-Martin, E.E., Kitidis, V., 2015. Satellite estimates of net community production indicate predominance of net autotrophy in the Atlantic Ocean. *Remote Sens. Environ.* 164, 254–269. <https://doi.org/10.1016/j.rse.2015.03.017>.
- Tzanatos, E., Raitos, D.E., Triantafyllou, G., Somarakis, S., Tsonis, A.A., 2014. Indications of a climate effect on Mediterranean fisheries. *Climatic Change* 122, 41–54. <https://doi.org/10.1007/s10584-013-0972-4>.
- Veitch, J.A., Penven, P., 2017. The role of the Agulhas in the Benguela Current system: a numerical modeling approach. *J. Geophys. Res. Oceans* 122, 3375–3393.
- Zantsi, B., 2013. The Chokka squid fishery in South Africa: review of the 2005 policy [final project]. <https://www.grocentre.is/static/gro/publication/279/document/bongiwe12prf.pdf>.
- Zhang, C., Hu, C., Shang, S., Müller-Karger, F.E., Li, Y., Dai, M., Huang, B., Ning, X., Hong, H., 2006. Bridging between SeaWiFS and MODIS for continuity of chlorophyll-a concentration assessments off Southeastern China. *Remote Sens. Environ.* 102, 250–263. <https://doi.org/10.1016/j.rse.2006.02.015>.